Contrib Mineral Petrol (2006) 152:275–294
DOI 10.1007/s00410-006-0101-8

ORIGINAL PAPER

A subduction wedge origin for Paleoarchean peridotitic diamonds and harzburgites from the Panda kimberlite, Slave craton: evidence from Re–Os isotope systematics

K. J. Westerlund · S. B. Shirey · S. H. Richardson ·
R. W. Carlson · J. J. Gurney · J. W. Harris

Received: 28 March 2005 / Accepted: 24 March 2006 / Published online: 4 July 2006

Abstract An extensive study of peridotitic sulfide inclusion bearing diamonds and their prospective harzburgitic host rocks from the 53 Ma Panda kimberlite pipe, Ekati Mine, NWT Canada, has been undertaken with the Re–Os system to establish their age and petrogenesis. Diamonds with peridotitic sulfide inclusions have poorly aggregated nitrogen (< 30% N as B centers) at N contents of 200–800 ppm which differs from that of chromite and silicate bearing diamonds and indicates residence in the cooler portion of the Slave craton lithospheric mantle. For most of the sulfide inclusions, relatively low Re contents (average 0.457 ppm) and high Os contents (average 339 ppm) lead to extremely low $^{187}Re/^{188}Os$, typically < < 0.05. An age of 3.52 ± 0.17 Ga (MSWD = 0.46) and a precise initial $^{187}Os/^{188}Os$ of 0.1093 ± 0.0001 are given by a single regression of 11 inclusions from five diamonds that individually provide coincident internal isochrons. This initial Os isotopic composition is 6% enriched in ^{187}Os over 3.5 Ga chondritic or primitive mantle. Sulfide inclusions with less radiogenic initial Os isotopic compositions reflect isotopic heterogeneity in diamond forming fluids. The harzburgites have even lower initial $^{187}Os/^{188}Os$ than the sulfide inclusions, some approaching the isotopic composition of 3.5 Ga chondritic mantle. In several cases isotopically distinct sulfides occur in different growth zones of the same diamond. This supports a model where C–O–H–S fluids carrying a radiogenic Os signature were introduced into depleted harzburgite and produced diamonds containing sulfides conforming to the 3.5 Ga isochron. Reaction of this fluid with harzburgite led to diamonds with less radiogenic inclusions while elevating the Os isotope ratios of some harzburgites. Subduction is a viable way of introducing such fluids. This implies a role for subduction in creating early continental nuclei at 3.5 Ga and generating peridotitic diamonds.

Communicated by T. L. Grove

Electronic Supplementary Material Supplementary material is available for this article at http://dx.doi.org/10.1007/s00410-006-0101-8 and is accessible for authorized users.

K. J. Westerlund · S. H. Richardson · J. J. Gurney
Department of Geological Sciences,
University of Cape Town,
Private Bag, Rondebosch 7700, South Africa
e-mail: kjw@geology.uct.ac.za
e-mail: shr@geology.uct.ac.za

J. J. Gurney
e-mail: jjg@geology.uct.ac.za

S. B. Shirey (✉) · R. W. Carlson
Department of Terrestrial Magnetism,
Carnegie Institution of Washington,
5241 Broad Branch Road, N.W.,
Washington, DC 20015, USA
e-mail: shirey@dtm.ciw.edu

R. W. Carlson
e-mail: carlson@dtm.ciw.edu

J. W. Harris
Department of Geographical and Earth Sciences,
University of Glasgow, Glasgow G12 8QQ, UK
e-mail: J.Harris@ges.gla.ac.uk

Present address: K. J. Westerlund
Swedish Geological/Hifab AB,
P.O. Box 19090, 10432 Stockholm, Sweden
e-mail: karl.westerlund@hifab.se

Introduction

The cratonic lithospheric mantle reaches depths of >200 km (Jordan 1979, 1981, 1988; Rudnick and Nyblade 1999) and its highly refractory peridotite likely formed in response to large-volume melt extraction (e.g., Boyd 1989) predominantly in the Archean (Pearson et al. 1995b; Carlson et al. 1999b; Irvine et al. 2003). Low-Ca garnet harzburgite is generally a minor constituent of the dominantly lherzolitic cratonic mantle ‘‘keels’’ (e.g., Schulze 1995) but hosts the relatively abundant harzburgitic paragenesis diamonds (Gurney 1989) that in the case of the Kaapvaal craton were dated as Paleoarchean (Richardson et al. 1984). The petrogenetic relationship between harzburgite and harzburgitic diamonds is still poorly known. Recent diamond finds in the Slave craton of the Northwest Territories of Canada have provided new suites of peridotite and eclogite xenoliths and diamonds that can be used to explore diamond-host relationships and cratonic lithosphere evolution.

We have examined harzburgitic garnet nodules (± orthopyroxene ± olivine ± chromite) and a large suite of peridotitic sulfide inclusions in diamonds from the 53 Ma old Panda kimberlite (Carlson et al. 1999a; Creaser et al. 2004; Nowicki et al. 2004) for their composition and Re–Os isotopic systematics. Host diamonds were examined for their cathodoluminescence patterns, their N content, their N aggregation states, and the relationship of multiple inclusion bearing diamonds to these features. The goals of this study are to understand how the diamonds are formed in their putative host harzburgite, to date lithosphere depletion and diamond formation, and to elucidate the geological processes that created depleted lithospheric mantle in the geologic setting of the Slave craton.

Geologic setting

The geologic setting, lithologies, and diamond distribution within the Panda kimberlite pipe have been recently described by Nowicki et al. (2004) and Dyck et al. (2004). A precise phlogopite Rb–Sr age of 53.2 ± 0.3 Ma for the Panda kimberlite has been determined by Creaser et al. (2004). Diamonds were collected from run-of mine production of the Panda kimberlite pipe, in June 2000 (Westerlund 2005). Since 2002, Panda diamond feed has been blended with production from other Ekati pipes such as Misery, Koala, and Koala North (Dyck et al. 2004). Thus the pre-2002 date of diamond sampling assures that all specimens analyzed here are from only the Panda pipe.

Recent studies (Bleeker 2003; Davis et al. 2003b; Aulbach et al. 2004) have synthesized the structural and tectonic framework of the Slave craton. Briefly, the Slave craton is an asymmetric construct of the Neoarchean to Eoarchean (2.6–4.0 Ga) Central Slave Basement Complex on the west and the Neoarchean (2.6–2.7 Ga) eastern Slave arc on the east (subdivisions and terms for the Archean Eon after the recommendations of the International Commission on Stratigraphy; Robb et al. 2004). The Panda kimberlite intrudes the eastern Slave arc, 100 km to the east of the putative suture that separates the two halves of the craton. The Panda kimberlite is located close to a major geochemical boundary in initial Nd isotopic composition of granitoids between those that were derived from mid-crustal sources containing components of older Central Slave Basement Complex crust and those whose sources were juvenile (Davis and Hegner 1992; Davis et al. 2003b).

The central Slave craton lithospheric mantle is unusual in that it appears to be compositionally (e.g., Davis et al. 2003b) and perhaps temporally (Irvine 2002) layered. Peridotite xenoliths (Kopylova and Russell 2000) and garnet macrocrysts (Griffin et al. 1999) from the upper 150 km are on average highly depleted in magmaphile trace elements indicating the presence of a relatively shallow ‘‘ultra-depleted layer’’ (UDL) thought to have a ratio of harzburgite to lherzolite as high as 1.5 (Griffin et al. 1999). Deeper parts of the central Slave lithosphere appear to have a lower harzburgite to lherzolite ratio of about 0.25 (Griffin et al. 1999).

Samples and analytical techniques

Seven peridotitic xenoliths were selected for electron microprobe analysis of their constituent olivine, orthopyroxene, garnet, and chromite and laser ablation ICPMS analysis of their garnet (eTable 1). These analyses were carried out at the Department of Geological Sciences, University of Cape Town (UCT) with analytical procedures described fully in Westerlund (2005).

The diamonds hosting the PD series of sulfides (Tables 1, 2, 3) were selected for study because of their approximately one carat size, white or near-white color, octahedral or slightly distorted or resorbed octahedral morphology, and the presence of large or multiple inclusions. PA series diamonds may represent a different population(s) with sizes 0.12–0.20 carats per stone, including both brown and colorless specimens, and having octahedral, macle, and irregular shapes.

Table 1 Average N content, N aggregation characteristics, and model temperature for Panda PD series diamond plates

Sample	N (ppm)	%N as B	*T* (°C)	*n*
PD2	537	15.7	1,088	14
PD3	506	19.0	1,094	18
PD4	516	17.8	1,092	12
PD5	477	10.1	1,078	15
PD6	419	15.3	1,093	9
PD7	273	14.6	1,101	11
PD9	384	17.0	1,098	14
PD10	292	15.6	1,101	15

N is the average nitrogen content of the diamond plate. %N as B is the percent of total N present as B aggregates. *T* is the temperature for a mantle residence time of 3.5 billion years, *n* is the number of traverse points

Table 2 Major element composition of sulfide inclusions in Panda diamonds

Sample	Fe (wt%)	Ni (wt%)	Cu (wt%)	Co (wt%)	S (wt%)
PD2a	40.0	25.2	0.1	0.4	34.2
PD2b	40.1	24.9	0.9	0.0	34.1
PD3a	42.2	22.3	0.0	1.1	34.4
PD3b					
PD4a					
PD4b					
PD4c	41.6	23.1	0.7	0.5	34.2
PD4d	39.7	25.6	0.0	0.5	34.2
PD4e					
PD4f	37.8	27.9	0.0	0.4	33.9
PD5	41.9	22.2	1.8	0.4	33.7
PD6a	43.5	20.7	0.9	0.3	34.6
PD6b	41.9	22.7	0.6	0.3	34.4
PD7a					
PD7b	42.2	22.5	0.0	0.5	34.7
PD9a	51.5	11.3	0.3	0.3	36.5
PD9b	41.9	22.9	0.0	0.5	34.6
PD9c	40.3	25.1	0.0	0.2	34.5
PD10a	49.6	13.8	0.0	0.2	36.4
PD10b	40.6	24.6	0.0	0.4	34.4
PA87c	42.7	21.9	0.2	0.5	34.7
PA89a	41.6	22.8	1.2	0.4	34.0
PA91a	41.3	22.8	1.8	0.5	33.6
PA92a	40.5	23.7	2.0	0.5	33.3
PA93a	31.4	34.7	1.4	0.5	31.9
PA94a	43.3	21.1	0.6	0.4	34.6
PA95a	40.6	24.3	0.5	0.5	34.1
PA96a	40.6	24.4	0.4	0.4	34.2
PA97a	46.5	17.1	0.7	0.4	35.2
PA98a/1	39.9	25.4	0.0	0.5	34.2
PA98a/2	42.5	22.1	0.4	0.5	34.5

Compositions were determined by the method of standard addition using solution nebulization on an Axiom ICP–MS at the Department of Terrestrial Magnetism. Only Fe, Ni, Cu, and Co were analyzed; S is determined by difference. These solutions are full bulk analyses of the inclusions analyzed for Re–Os presented in Table 3

PA series sulfides were broken straight out of their diamond hosts whereas PD series diamonds were cut into plates and analyzed at UCT in traverses for nitrogen content and aggregation using Fourier transform infra-red (FTIR) absorption analysis prior to liberating the sulfides. Again, these methods are described in detail in Westerlund (2005).

Sulfides from the PD series were carefully extracted through gentle cracking of diamond plates in an attempt to completely recover each grain. In most cases the whole sulfide was liberated intact. Some sulfides broke up into multiple pieces and PD5 shattered into more than 20 fragments. Sulfides from the PA series diamonds were also subject to fragmentation but unfractured grains were analyzed wherever possible.

Sulfide inclusions and harzburgites were analyzed for their Re–Os and related systematics at the Department of Terrestrial Magnetism, Carnegie Institution of Washington, following methods developed by Shirey and Walker (1995), Pearson et al. (1998), Carlson et al. (1999b), and Shirey et al. (2000) as detailed in the eAppendix.

Xenolith petrography, mineral compositions, and geothermobarometry

The xenoliths were purple garnet nodules measuring about 1–4 cm across that commonly carried poikilitic orthopyroxene (< 20 modal %) and olivine (< 10 modal %; one nodule was devoid of olivine). Most xenoliths had modal orthopyroxene/olivine >> 1. Accessory chromite was present in three of the samples whereas sulfide was never observed. Based on the absence of clinopyroxene and mineral major element compositions (eTable 1) that are typical of cratonic harzburgite the nodules are from now on referred to as harzburgites. Like other garnets from diamondiferous kimberlites, the garnets as shown in Fig. 1a fall cleanly into the harzburgitic field and are extremely Cr-rich. Garnet from three of the nodules shows sinusoidal REE_N (rare earth element concentrations normalized to chondrite values from McDonough and Sun 1995) patterns (Fig. 1b). The trace element concentrations and sinusoidal REE_N patterns are similar to those of previously analyzed harzburgitic garnets found as inclusions in diamonds, macrocrysts, and xenoliths (e.g., Shimizu and Richardson 1987; Griffin et al. 1992; Hoal et al. 1994; Stachel and Harris 1997; Stachel et al. 1998) as well as macrocrysts derived from the UDL (Griffin et al. 1999).

The pressures and temperatures estimated using the Harley (1984) geothermometer in combination with the geobarometers of Nickel and Green (1985) and MacGregor (1974) (the latter as formulated by Finnerty and Boyd 1984) are 47–52 kbars/910–990°C and 42–49 kbars/900–1,000°C, respectively. Applying the

Table 3 Sample weights, Re–Os concentrations, and Os isotopic compositions for sulfide inclusions in Panda diamonds

Sample	Iso	Wt (μg)	Re (ppm)	Os (ppm)	^{187}Re/^{188}Os	^{187}Os/^{188}Os	Os Init	γ_{Os}	T_{MA}	T_{RD}
PD2a	I	9.0	0.266	152.9	0.00835 ± 0.00018	0.10987 ± 0.00017	0.10937	5.9	2.7	2.7
PD2b	I	5.7	0.263	319.9	0.00391 ± 0.00014	0.10948 ± 0.00037	0.10924	5.7	2.7	2.7
PD3a	I	28.1	0.213	35.85	0.02856 ± 0.00026	0.11098 ± 0.00029	0.10925	5.7	2.7	2.5
PD3b	I	0.7	0.355	53.70	0.0318 ± 0.0064	0.11116 ± 0.00046	0.10924	5.7	2.7	2.5
PD4		12.4	0.453	16.04	0.136 ± 0.022	0.1167 ± 0.0012	0.10851	5.0	2.5	1.8
PD4a		1.9	0.756	14.31	0.2542 ± 0.0089	0.11910 ± 0.00048	0.10373	0.4	3.4	1.4
PD4b	I	1.3	0.518	23.80	0.1048 ± 0.0078	0.11589 ± 0.00071	0.10955	6.0	2.4	1.9
PD4c	I	3.2	0.348	9.931	0.1689 ± 0.0076	0.11956 ± 0.00039	0.10935	5.8	2.2	1.4
PD4d	I	3.6	0.449	28.28	0.07648 ± 0.0043	0.11406 ± 0.00082	0.10944	5.9	2.5	2.1
PD4e		0.5	0.942	13.74	0.3300 ± 0.0035	0.11586 ± 0.00074	0.09591	-7.2		1.9
PD4f		3.5	0.292	13.00	0.1084 ± 0.0053	0.11737 ± 0.00048	0.11082	7.3	2.2	1.7
PD5		12.0	0.290	350.1	0.00399 ± 0.00013	0.10930 ± 0.00016	0.10906	5.6	2.8	2.7
PD6a		6.8	0.743	73.84	0.00484 ± 0.00022	0.10913 ± 0.00019	0.10884	5.3	2.8	2.8
PD6b		1.9	0.848	2142	0.00190 ± 0.00006	0.10928 ± 0.00013	0.10917	5.7	2.8	2.7
PD7a		1.0	0.148	144.5	0.0049 ± 0.0017	0.10925 ± 0.00031	0.10895	5.5	2.8	2.7
PD7b		2.8	0.207	271.25	0.00368 ± 0.00032	0.10903 ± 0.00040	0.10881	5.3	2.8	2.8
PD9a		6.8	0.433	421.0	0.00494 ± 0.00021	0.10953 ± 0.00012	0.10923	5.7	2.7	2.7
PD9b		2.9	0.329	346.5	0.00457 ± 0.00026	0.10928 ± 0.00024	0.10900	5.5	2.8	2.7
PD9c		2.7	0.701	772.2	0.00440 ± 0.00063	0.10919 ± 0.00017	0.10892	5.4	2.8	2.8
PD10a	I	1.7	0.318	81.87	0.0187 ± 0.0017	0.11056 ± 0.00040	0.10943	5.9	2.7	2.6
PD10b	I	1.3	0.579	3805	0.00092 ± 0.00011	0.10925 ± 0.00024	0.10919	5.7	2.8	2.7
PA87c		6.7	0.074	4.296	0.08327 ± 0.00083	0.11568 ± 0.00045	0.11065	7.1	2.3	1.9
PA89a		6.6	0.834	28.33	0.1417 ± 0.0014	0.11997 ± 0.00027	0.11141	7.8	1.9	1.3
PA91a		27.9	1.586	6.487	1.192 ± 0.003	0.21230 ± 0.00029	0.14024	35.7		
PA92a		5.7	1.320	31.74	0.2007 ± 0.0014	0.13126 ± 0.00022	0.11913	15.3		
PA93a		6.3	0.500	89.53	0.02681 ± 0.00046	0.11128 ± 0.00017	0.10966	6.1	2.6	2.5
PA94a		6.0	2.420	67.98	0.1716 ± 0.0011	0.12353 ± 0.00030	0.11315	9.5	1.4	0.8
PA95a		46.2	0.376	41.86	0.04318 ± 0.00033	0.11065 ± 0.00058	0.10804	4.6	2.8	2.6
PA96a		16.1	0.323	95.70	0.01626 ± 0.00017	0.11009 ± 0.00018	0.10911	5.6	2.7	2.6
PA97a		3.0	2.659	0.824	19.77 ± 0.15	2.228 ± 0.014	1.033			
PA98a/1	I	3.9	0.601	63.39	0.0456 ± 0.0010	0.11187 ± 0.00029	0.10911	5.6	2.7	2.4
PA98a/2	I	11.6	0.657	65.90	0.04800 ± 0.00036	0.11214 ± 0.00024	0.10924	5.7	2.7	2.4

PD4 is a weighted recombination of six inclusions (4a–f) from diamond PD4 (see text). Samples with the designation of I in column Iso regress to yield a Re–Os isochron age of 3,523 ± 170 Ma with a ^{187}Os/^{188}Os IR of 0.1093 ± 0.0001 (MSWD = 0.46; Isoplot Model 1; probability = 0.90; Ludwig 2003). Errors given are two-sigma as estimated from all sources of error. For ^{187}Re/^{188}Os this is dominated by variability in the 100 fg Re blank of ± 50 fg and for ^{187}Os/^{188}Os this is dominated by mass spectrometry in-run statistics. Os Init, γ_{Os}, T_{MA}, and T_{RD} are calculated using the 3,523 Ma isochron age and a ^{187}Re decay constant of 1.666×10^{-11} year^{-1}. γ_{Os} is the deviation in % of the initial Os isotopic composition from a specified reference reservoir, in this case the primitive mantle reservoir of Meisel et al. (2001). This reservoir had a ^{187}Os/^{188}Os 4,557 Ma ago of 0.09531, a present day value of 0.1296, and requires a ^{187}Re/^{188}Os of 0.43464 to evolve from the former to the latter. T_{MA} is the 'time of mantle extraction'' model age and T_{RD} is the ''time of rhenium depletion'' model age as defined in Walker et al. (1989) and Shirey and Walker (1998). In this table, both use the Meisel et al. (2001) primitive mantle composition. Value omitted where negative or older than the age of the Earth

O'Neill and Wood (1979) geothermometer in combination with the same geobarometers yields pressures and temperatures of 43–47 kbars/870–980°C and 39–48 kbars/840–990°C, respectively. The Ni-in-garnet thermometer of Ryan et al. (1996) gives a similar temperature range of 910–1,013°C. Combining the O'Neill and Wood (1979) geothermometer with the Brey and Kohler (1990) Al-in-opx geobarometer gives 39 kbars/950°C for one of the xenoliths whereas three of the xenoliths give very low pressures and temperatures (20–28 kbars/730–795°C) and for two of the xenoliths, the thermometer and barometer do not converge. This could possibly be a result of the comparatively complex nature of the Brey and Kohler (1990) barometer as applied to the extreme mineral compositions of the xenoliths (high-Cr/low-Ca garnets and very low Al orthopyroxene). Alternatively, the minerals are not in equilibrium, which could result from storage in a comparatively cool mantle regime in order to preserve the chemical disequilibrium. Menzies et al. (2004) showed that the geotherm in the area of the Panda kimberlite intersects the diamond stability field (Kennedy and Kennedy 1976) at approximately 42 kbars and 900°C, and further that the UDL reaches depths of about 150 km corresponding to a temperature of about 1,000°C. Thus, the estimations for the current xenoliths, despite disagreements between geothermobarometers, are indicative of an origin from the UDL within the diamond stability field or straddling the graphite/diamond stability boundary.

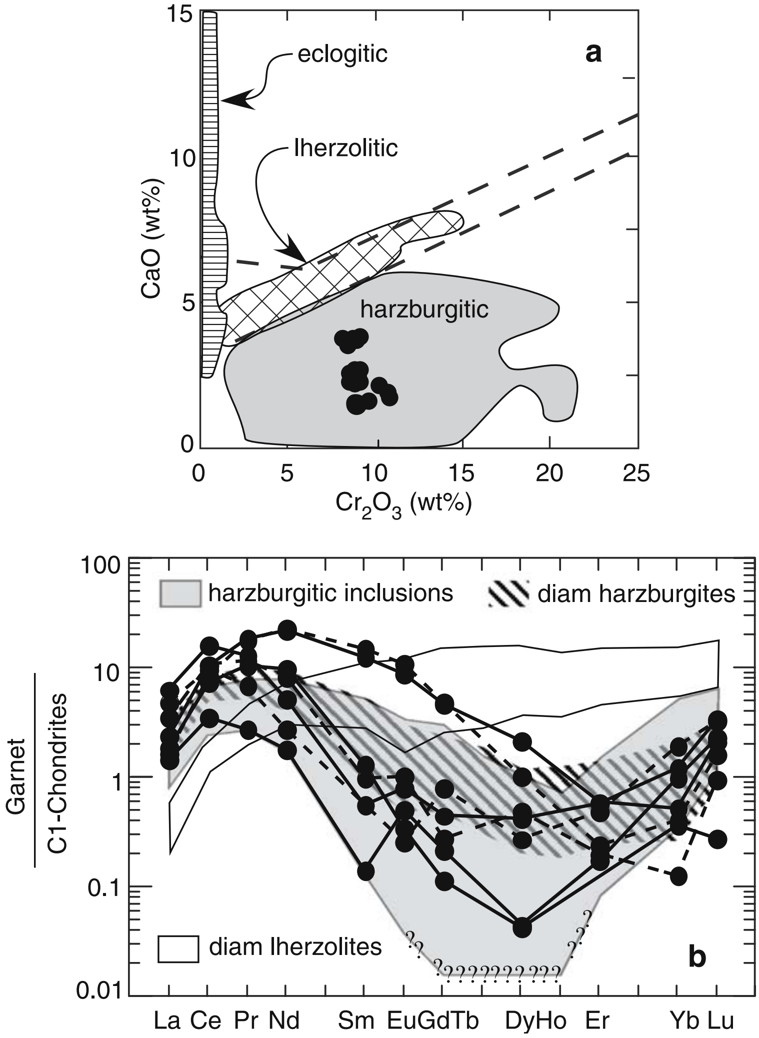

Fig. 1 Garnet compositions for Panda harzburgites. **a** The high Cr_2O_3, low CaO content typical of cratonic garnets from diamond-bearing regions of the cratonic lithosphere (e.g., Gurney and Switzer 1973; Sobolev et al. 1973; Stachel et al. 1998; Taylor and Anand 2004). **b** The sinusoidal REE pattern typical of garnet that has experienced a multistage evolutionary history of melt depletion followed by fluid enrichment and a second melt depletion (e.g., Shimizu and Richardson 1987; Stachel et al. 1998; Taylor and Anand 2004). Fields in both figures are constructed from a database of Stachel and Harris (1997) and Stachel et al. (1998)

Nitrogen content and aggregation of the sulfide inclusion bearing diamonds

Table 1 presents the average nitrogen content, nitrogen aggregation, and mantle residence temperature for each of the eight plates analyzed; eTable 2 presents each individual data point and a discussion of the aggregation process and the estimation of temperatures. Most of the sulfide and chromite bearing Panda diamonds (this study and Stachel et al. 2003) have little aggregated nitrogen whereas the majority of the silicate bearing diamonds carry nitrogen that is considerably more aggregated (Fig. 2). Further, the chromite bearing diamonds generally have lower nitrogen content than the sulfide bearing diamonds (see Westerlund 2005 for more detail). While the age(s) of the Stachel et al. (2003) diamonds is unknown, the present data are suggestive of an association dominated by chromite and sulfide bearing diamonds with a time-averaged mantle residence temperature (T_{MR}) of 1,050–1,100°C (Fig. 2). These resided at relatively shallow depths in the lithosphere and a distinct diamond population with dominantly silicate inclusions resided deeper in the lithosphere. Figure 2 also shows the nitrogen content of peridotitic diamonds from all available literature data. Note that the bulk of Panda sulfide bearing diamonds fall on the high nitrogen content side of the bulk of worldwide peridotitic diamonds.

The carbon ($^{13}C/^{12}C$) and nitrogen ($^{15}N/^{14}N$) isotopic compositions of the Panda diamond plates have been analyzed with the Cameca IMS6F Ion Microprobe at the Carnegie Institution of Washington (e.g., Hauri et al. 2002) and are presented in detail elsewhere (Westerlund et al. 2003; Westerlund 2005). On average, the $\delta^{13}C$ for Panda diamonds is –5‰ and the average $\delta^{15}N$ is –17‰ placing them within the field for peridotitic diamonds worldwide although on the isotopically light side of the nitrogen isotopic distribution (e.g., Fig. 57 in Pearson et al. 2003).

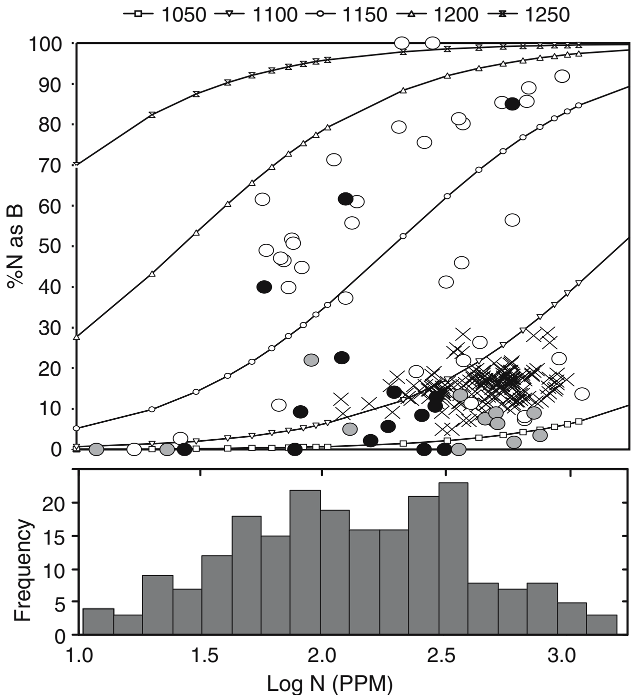

Fig. 2 Nitrogen aggregation (the percentage of total nitrogen present as B aggregates) versus the log of nitrogen content (ppm) for the Panda PD series diamonds (*crosses*) herein and in Westerlund (2005). Also shown for comparison are other Panda diamonds from Stachel et al. (2003) carrying sulfide inclusions (*gray*), chromite inclusions (*black*) and silicate inclusions (*white*). *Curves* represent isotherms (°C) for a mantle residence time of 3.5 billion years. A histogram of the nitrogen content of peridotitic diamonds worldwide is shown for reference (Pearson et al. 2003, Fig. 55). Note that the peridotitic sulfide-bearing diamonds from Panda cluster at the high-N-content end of the peridotitic diamond distribution closer to the mean log nitrogen content for eclogitic diamonds (2.78)

Physical characteristics, mineralogy, and composition of the sulfide inclusions

Eight of the diamonds contained multiple sulfide inclusions (Fig. 3; Table 3) and 31 sulfides were analyzed for their major element and Re–Os isotopic compositions. The sulfides have mostly irregular forms, sometimes with a broadly cubo–octahedral outline, and all grains were surrounded by thin ‘‘black rosette’’ fractures. The surfaces of the sulfides are commonly covered with minute diamond-induced features, such as triangular depressions, giving them a ‘‘frosty’’ appearance at low magnification, whereas some sulfides have partly or wholly smooth surfaces. Sulfide PA87c is distinct from the others with a highly symmetrical cubo–octahedral habit and very smooth surfaces. Most sulfides, particularly in the ‘‘frosted’’ areas, have a blue tinge to their color, typical of bornite whereas smooth surfaces have a pale yellow appearance typical of pentlandite or pyrrhotite.

Energy dispersive X-ray spectroscopy (EDS; eAppendix) has shown that the sulfides are dominated by pentlandite carrying about 20–25 wt% Ni and up to 6 wt% Co. Some analyses, mostly of external surfaces, yielded Cu levels of 2–11 wt% and up to 20 wt% in two analyses. The two latter gave Ni contents of 7 and 14 wt%, respectively. These compositions could reflect exsolved Co and Cu bearing phases, partially sampled together with pentlandite (in the case of the higher Ni–lower Cu analyses) on the outside surfaces of grains because bulk analyses have much lower Cu and Co contents (see below). Six analyses from PD5, PA93, and PA98a/2 (two from each sulfide) together yielded compositional ranges of S = 2–11 wt%, Fe = 50–85 wt%, Ni = 10–25 wt%, Co = 0–6 wt%, and Cu = 0–20 wt%. The analyses that show the lowest S contents (2–3 wt%) are from distinct zones as apparent in back-scattered electron images whereas the other analyses represent scans across boundaries to a sulfide phase. This indicates the presence of Fe-Ni-Cu–Co alloy in at least some of the grains. For the sake of simplicity, the inclusions are referred to as sulfide inclusions below even though alloy was identified in three of the inclusions.

Major element compositions of the Panda bulk sulfides (Table 2) do not display these extremes in Cu (0–2 wt%) and Co (0–0.5 wt%) content and with the exception of three samples they have high Ni contents (20.7–34.7 wt%). On a Fe–Ni–S ternary diagram (Fig. 4) they plot toward pentlandite composition, well within the liquid field and away from monosulfide solid solution (mss) for phase relations near 1,100°C (Ebel and Naldrett 1997). At lower temperatures near 900°C, mss extends across the Fe–Ni join (Fig. 4; Karup-Moller and Mackovicky 1998).

Re, Os, and Ni contents and paragenesis

The sulfide inclusions have high Os content and span a very large range in Os concentration from 0.82 to 3,800 ppm. They also have a relatively large range in Re concentration from 0.074 to 2.66 ppm (Table 3). Multiple sulfides from individual diamonds often differ by a factor of 2 in Re content and by a factor of 2 or 3 in Os content (e.g., PD10). The high Os content is fully supported by their high Ni content and is distinctly different from the lower Os, lower Ni eclogitic inclusions from the Kaapvaal craton (Fig. 5a) studied previously by Richardson et al. (2001; 2004). This corroborates the suggestion of Pearson et al. (1998) and Pearson and Shirey 1999 that Os content may be as

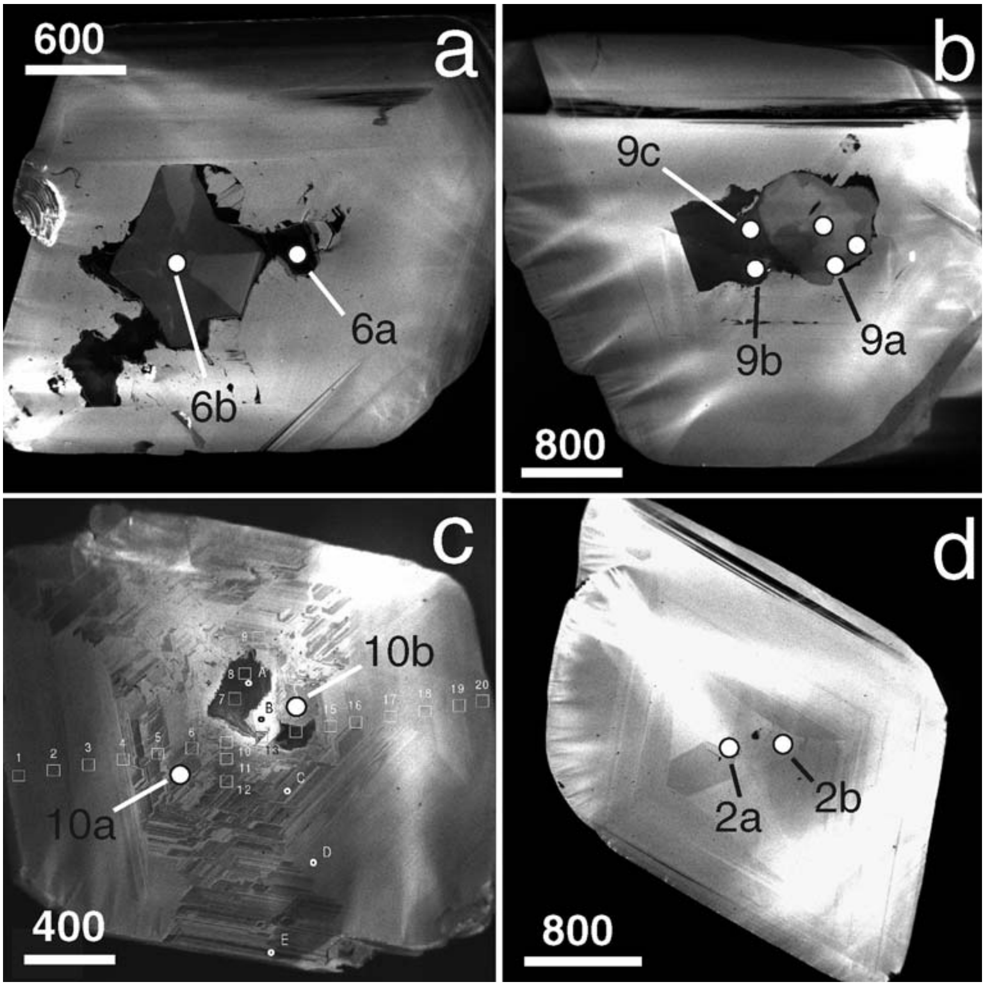

Fig. 3 Cathodoluminescence images of four Panda diamond plates (PD6, PD9, PD10, and PD2, respectively; length scales in microns). The positions of sulfide inclusions in these diamonds are shown by *white spots* that are labeled for reference to Table 3 and Figs. 7 and 8. Collectively, the diamonds display at least three phases of growth. The different concentration and isotopic compositions of these inclusions (Table 3) support isotopically distinct fluids and Re–Os fractionation during diamond growth

indicative as Ni when establishing sulfide inclusion paragenesis.

Discussions in the literature of sulfide inclusion paragenesis using Ni content (Deines and Harris 1995; Pearson and Shirey 1999) have suggested that eclogitic versus peridotitic sulfide inclusions show a gap in Ni content between 8 and 16 wt% chiefly based on the compositions of 16 sulfides examined in 1983 from the Siberian craton (e.g., Gurney 1989). A larger suite of sulfides (> 100) examined by Deines and Harris (1995) showed some inclusions with intermediate Ni content and a separate inclusion paragenesis with Ni content of 10–15 wt% was suggested (Deines and Harris 1995). More than 60 inclusions have recently been analyzed by bulk dissolution methods (Fig. 5) and only 5 of the 60 fall in the intermediate Ni content range. Thus a separate intermediate Ni paragenesis is not supported by the data.

The high Ni and Os concentrations seen in these Panda sulfides (Tables 2, 3) indicate a peridotitic paragenesis (e.g., Bulanova et al. 1996; Pearson and Shirey 1999) chiefly because their typical Ni content of 23–26 wt% is an excellent match for both Siberian and Kaapvaal peridotitic sulfide inclusions as is their typical Os content of 10^4–10^6 ppb (Pearson and Shirey 1999; Pearson et al. 2003). We note that the typical Ni/Fe of Panda sulfides (0.6; Table 2) further supports the peridotitic paragenesis because a Ni/Fe ratio of 0.6 would be expected for a sulfide in equilibrium with a depleted lithospheric mantle olivine such as in the Panda xenoliths ($Fo_{92.5}$; eTable 1) for a $K_D\{X_{Ni}/X_{Fe})_{sulfide}/(X_{Ni}/X_{Fe})_{olivine}\}$ of 20 at 1,100°C (e.g., Naldrett 1989; Deines and Harris 1995).

The Re and Os concentrations of the analyzed sulfide inclusions are shown in Fig. 6 together with other peridotitic sulfide inclusions, the host harzburgites, other cratonic peridotites, the primitive mantle (fertile lherzolite), komatiites, and komatiitic sulfides. The high Os concentrations displayed by most of the Panda sulfides coincide with very low Re contents and give very low Re/Os ratios that range down to 0.0002 (and $^{187}Re/^{188}Os < 0.001$). An inverse correlation between $^{187}Re/^{188}Os$ and Ni (Fig. 5b), which is as strong as the positive correlation between Os and Ni (Fig. 5a),

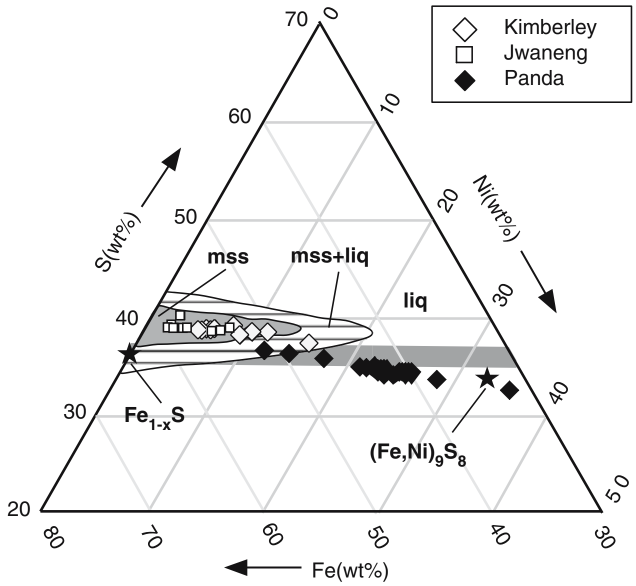

Fig. 4 Bulk major element composition of whole-grain, Panda peridotitic sulfide inclusions compared to eclogitic inclusions from Kimberley (Richardson et al. 2001) and Jwaneng (Richardson et al. 2004). A portion of the Fe–Ni–S ternary diagram with Cu-absent phase relations around 1,100°C is shown as fields of monosulfide solid solution (mss), mss + liquid, and sulfide liquid (Ebel and Naldrett 1997). The low-temperature stable minerals pyrrhotite ($Fe_{1-x}S$) and pentlandite {$(Fe,Ni)_9S_8$} are shown for reference. The subhorizontal, wide, *gray line* represents {$(Fe,Ni)_{1-x}S$} solid solution (mss) that is present at ≤ 900°C across the entire Fe–Ni join (Karup-Moller and Mackovicky 1998)

shows that in sulfide inclusions the chief control on Re/Os ratio is Os content, as seen in most igneous rocks (Shirey and Walker 1998). The Re/Os ratios for most of the sulfides are substantially lower than that estimated for the fertile mantle (Meisel et al. 2001) and also significantly lower than the Re/Os ratios displayed by most cratonic peridotites and previously analyzed peridotitic sulfide inclusions. Some Panda sulfides have slightly elevated Re contents (up to 2.66 ppm) compared to the rest and two of these have low Os concentrations so that their high Re/Os ratios mirror those of komatiite and eclogite/basalt respectively. Sample PA87c has relatively low concentrations of both Re and Os (0.074 and 4.3 ppm, respectively; Fig. 6), which makes it distinct from the rest of the sulfides. Nevertheless, its Ni and Os content and Re/Os ratio are characteristic of a peridotitic paragenesis.

Re and Os may partition differently during late-stage exsolution of chalcopyrite from a monosulfide solution (Richardson et al. 2001) and there is also experimental evidence for a higher monosulfide solution/sulfide melt partition coefficient for Os compared to Re (Fleet et al. 1999; Brenan 2002). Further, Os readily forms alloys with other platinum group elements in podiform chromites (e.g., Ahmed and Arai 2003) and has a higher affinity for alloy compared to Re. Thus, the large ranges in Re and particularly in Os concentration observed even for sulfides from individual diamonds may be governed by the modal mineralogy of the grains. The unusually high concentrations of Os in many of the grains could have resided mostly in alloy, even if the SEM analysis has

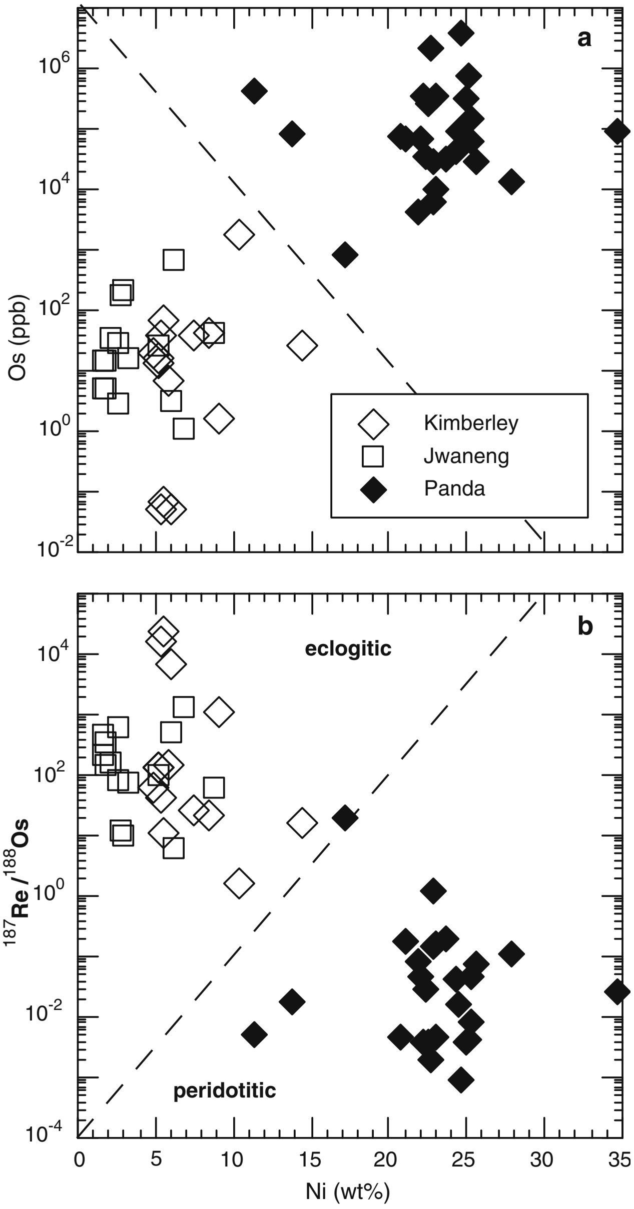

Fig. 5 **a** Os contents (in parts per billion) versus Ni contents (in wt%) comparing eclogitic sulfide inclusions from Kimberley and Jwaneng to peridotitic inclusions from Panda. **b** $^{187}Re/^{188}Os$ versus Ni contents for the same inclusions. Data sources as given in Fig. 4. Note the almost complete lack of overlap between the eclogitic and peridotitic suites

Table 4 Re and Os concentrations, and Os isotopic compositions for harzburgites

Sample	Re (ppb)	Os (ppb)	^{187}Re/^{188}Os	^{187}Os/^{188}Os	Os Init	γ_{Os}	T_{MA}	T_{RD}
PH1	0.0137	2.54	0.0259 ± 0.0013	0.10633 ± 0.00031	0.10476	1.4	3.3	3.1
PH2	0.0142	1.05	0.0647 ± 0.0032	0.10802 ± 0.00036	0.10411	0.8	3.4	2.9
PH15	0.0096	3.76	0.0122 ± 0.0006	0.10913 ± 0.00017	0.10839	4.9	2.8	2.8
PH16	0.0155	3.64	0.0205 ± 0.0010	0.10890 ± 0.00014	0.10766	4.2	2.9	2.8
PH17	0.0243	5.08	0.0230 ± 0.0015	0.10857 ± 0.00021	0.10718	3.7	3.0	2.8
PH18	0.0048	0.63	0.0370 ± 0.0019	0.11012 ± 0.00073	0.10789	4.4	2.9	2.6
PH19	0.0051	1.17	0.0211 ± 0.0011	0.10776 ± 0.00015	0.10649	3.1	3.1	2.9

Errors given are two-sigma as estimated from the dominant source of error. For ^{187}Re/^{188}Os this is the error magnification on the Re isotope dilution determination or the estimated 0.5% total error in the measured ^{187}Re/^{188}Os, whichever is greater. For ^{187}Os/^{188}Os the error is given from mass spectrometry in-run statistics. Os Init, γ_O, T_{MA}, and T_{RD} are defined and calculated as in the caption of Table 3

confirmed the presence of alloy in only three of the inclusions.

The Os contents of the xenoliths (0.63–5.08 ppb; Table 4) are similar to those of other cratonic peridotites (Fig. 6). However, the Re contents (0.0051–0.0243 ppb) are among the lowest yet recorded for cratonic peridotites. As a result, the peridotites are similar to the diamond inclusion sulfides in that they show unusually low Re/Os ratios compared to other peridotitic mantle materials. However, the low Re/Os ratios of the harzburgites result from their exceptionally low Re contents in contrast to the low Re/Os ratios of the sulfide inclusions that result from their unusually high Os contents.

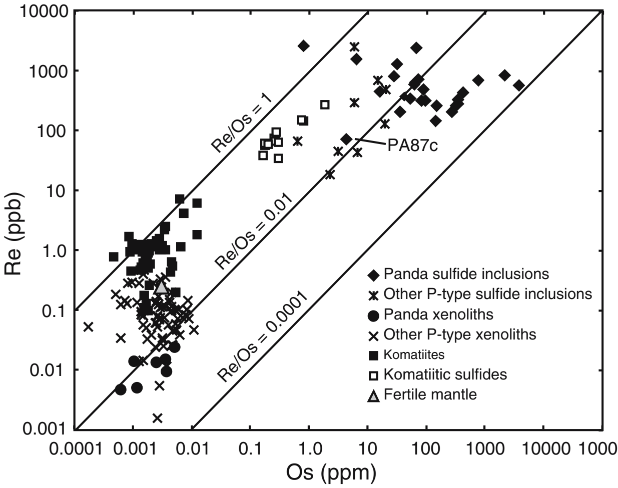

Fig. 6 Re and Os contents for the Panda harzburgites and sulfide inclusions in diamond compared to those of other cratonic peridotites, other peridotitic inclusion sulfides, komatiites, komatiitic sulfides, and fertile mantle. Literature data from Carlson and Irving (1994), Carlson et al. (1999b), Foster et al. (1996), Morgan (1986), Pearson et al. (1995a, b, 1998, 1999a, b), Puchtel et al. (2001), and Walker et al. (1988, 1989, 1991)

Re–Os isotope data

Isochron systematics and age implications

Twenty-one of the 31 sulfide inclusions are well enough correlated in a Re–Os isochron diagram ("main group" in Fig. 7) to be considered for isochron

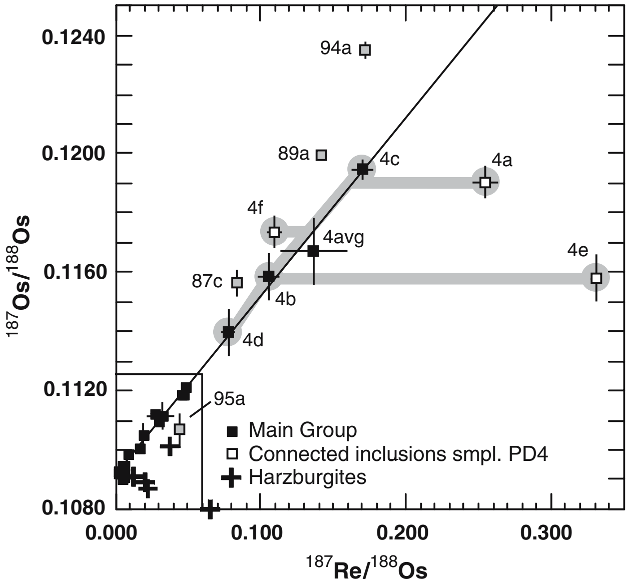

Fig. 7 Re–Os isochron diagram showing 28 of the 31 Panda sulfide inclusions studied and five of the seven Panda harzburgites (see inset expanded in Fig. 8). Regression of 11 inclusions from five diamonds produces an isochron (*black line*) with an age of 3,523 ± 170 Ma with an initial ^{187}Os/^{188}Os of 0.1093 ± 0.0001 (Isoplot Model 1; MSWD = 0.46; Ludwig 2003). Note the distinction between the "main group" (*black*) and those not on the main group (*shaded*) three of which (PA92a, PA91a, and PA97a) are off-scale. *Thick shaded lines* connect individual inclusions from diamond PD4, the weighted average analysis of which is shown as '4avg'. *Horizontal shaded lines* connect inclusions (4a, e, f) presumed to have been interconnected along 'rosette' fractures which underwent Re/Os fractionation upon exsolution during kimberlite eruption. *Shaded line* along regression connects three inclusions (4b, c, d) presumed to have been isolated (see text for details)

regression analysis. All diamonds in at least the PD series of this main group display similar growth morphology (Westerlund 2005) and nitrogen aggregation (Table 1; eTable 2) providing no indication that they comprise multiple diamond populations of variable formation age. Regression of all 21 samples shows scatter outside the experimental error (Age = 3,692 ± 200 Ma, MSWD = 3.3, Isoplot Model 3 Fit, Probability = 0; Ludwig 2003) due chiefly to sample PA93a and a group of six, tightly clustered inclusions that plot below the best-fit regression line (Fig. 8 and inset). Removing these seven inclusions from consideration leads to a statistically valid isochron comprising 14 inclusions that yields an age of 3,565 ± 150 Ma and an initial ^{187}Os/^{188}Os ratio of 0.1092 ± 0.0001 (MSWD = 0.64; Isoplot Model 1 Fit, Probability = 0.81). If only those diamonds are used whose inclusions show coherent internal age systematics which imply equilibrium (i.e., PD2, PD3, PD4, PD10, and PA98a), then an equally robust 11-point isochron is obtained with an age of 3,523 ± 170 Ma and an initial ^{187}Os/^{188}Os ratio of 0.1093 ± 0.0001 (MSWD = 0.46; Isoplot Model 1 Fit, Probability = 0.90). The large age uncertainty on these isochrons is a function of the very narrow range and low ^{187}Re/^{188}Os of the samples (0.00092–0.169).

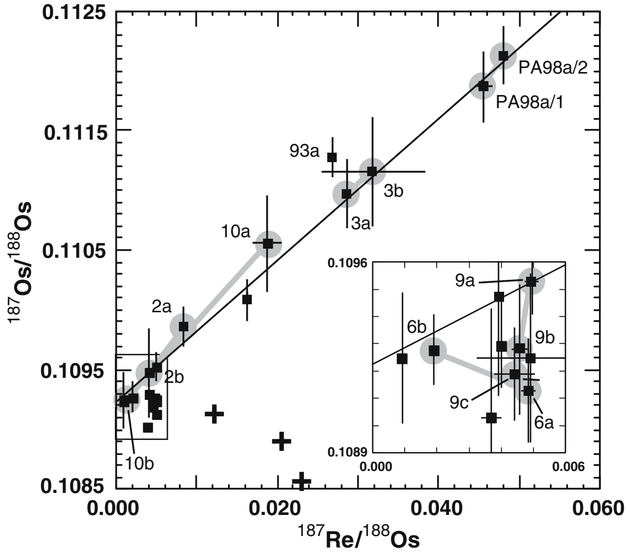

Fig. 8 Re–Os isochron diagram showing fit of samples (except 4b, c, and d which are shown in Fig. 7) that define the full 14-point 3,565 Ma isochron (see text for details). *Thick shaded lines* connect individual inclusions from the same diamond. Sample PA93a and the six samples below the isochron at low ^{187}Re/^{188}Os (see inset) are left off the regression. These six samples are excluded based on source isotopic heterogeneity as discussed in the text. Note that one harzburgite and sulfide PA95a are not plotted so that the inset may be shown. Some error bars on data points in the inset have been deleted from the full plot for clarity

The six sulfides below the isochron display similar and very low ^{187}Re/^{188}Os and clearly indicate Os isotopic heterogeneity in the sources of the diamonds. Two diamonds, PD6 and PD9 are the best examples of this because they carry multiple sulfides: one from each diamond conforms to the full 14-point isochron (Fig. 8) at the low ^{187}Re/^{188}Os end and the others are among the six sulfides with isotopic compositions that fall below the isochron (Fig. 8). Our attempt to correlate the position of these inclusions with diamond growth phases (e.g., Fig. 3a, b) is complicated by thickness of the diamond plates and the position of the inclusions below the luminescent surface of the diamond. It appears that these isotopically distinct sulfides are enclosed by early-formed, non- or weakly luminescent diamond that is in turn surrounded by strongly luminescent, inclusion free diamond. Two other diamonds, PD10 and PD2 display multiple inclusions that are confined to the strongly luminescent phase of diamond growth (Fig. 3c, d) which we interpret as similar to the later, outside, luminescent phase of diamond seen in PD6 and PD9 (Fig. 3a, b). In each of these diamonds, the inclusions have different ^{187}Re/^{188}Os and ^{187}Os/^{188}Os but the inclusions are co-linear within analytical uncertainties of the full 14-point isochron (Fig. 8). Such internal isochron behavior is also evident for the multiple inclusions from diamonds PD3, PD4, and PA98a (Figs. 7, 8; Table 3). This suggests that sulfide inclusions associated with the earliest phase of diamond growth at Panda are characterized by isotopic heterogeneity in ^{187}Os/^{188}Os as well as extremely low and constant ^{187}Re/^{188}Os, whereas sulfide inclusions associated with later phases of diamond growth are characterized by homogeneous initial ^{187}Os/^{188}Os but greater fractionation in ^{187}Re/^{188}Os.

Three diamonds with multiple inclusions (PD3, 5, and 7) do not fit the straightforward relationship between diamond growth zones and sulfide inclusion Re–Os systematics evident in the diamonds discussed above. Diamonds PD5 and 7 have inclusions off the isochron (within the low ^{187}Re/^{188}Os group; Fig. 8) but hosted by luminescent diamond. Diamond PD3 is complicated with a texturally simpler core region containing two inclusions and a texturally more complex core region containing no inclusions. Both of the inclusions are on the isochron at relatively high ^{187}Re/^{188}Os but only one of them is from non-luminescent diamond. The complex textural relationships for diamonds PD 3, 5, and 7 do not negate the relative growth phase versus Re–Os systematics outlined above for diamonds PD2, 6, 9, and 10 but simply imply that there must have been multiple pulses of fluids permeating the harzburgite from which diamonds grew and that the activators for diamond luminescence are not directly related to the Re–Os isotopic details of the included sulfides.

Sulfides from diamond PD4 (Fig. 7) require a more complicated interpretation. As mentioned above, three sulfides (4b, c, and d; Fig. 7) show internal isochron systematics (e.g., Age = 3,440 ± 580 Ma, MSWD = 0.074, Isoplot Model 1 Fit, Probability = 0.79) that follow the 3.57 Ga 14-point isochron or the 3.52 Ga 11-point isochron. Three other sulfides (4a, e, and f; Fig. 7) plot significantly to the right or left of these isochrons. We interpret the first three isochronous sulfides as forming far enough apart in the diamond so that their surrounding rosette fracture systems developed upon kimberlite eruption did not intersect. They remained isolated, closed systems and thus preserved 3.5 Ga age relations. The same interpretation applies to inclusions from diamonds PD2, PD3, PD10, and PA98a which each show internal two-point isochrons that were obtained from sulfides whose surrounding black rosette fracture systems were visibly separated from each other within the diamond. The second group of three sulfides from PD4 must have had intersecting rosette fractures that formed during transport to the surface in the kimberlitic magma. This would have allowed exchange of exsolved sulfide in the fractures and a change in Re/Os at a given ^{187}Os/^{188}Os in the sulfide grain recovered for analysis. Such a change in the partitioning of Re from Os according to sulfide mineralogy was first documented in a single inclusion from Kimberley (De Beers Pool) split into two parts and analyzed separately by Richardson et al. (2001). Incomplete recovery of inhomogeneous, exsolved sulfide grains either because pieces fracture off during cracking of the diamond or sulfide remained in the rosette fracture can lead to data points that plot far off the closed system trend as seen in inclusions 4a, e, and f. Interestingly, a weighted recombination of all PD4 inclusions leads to an average data point that plots on the closed system line albeit with very large errors.

The mantle model ages (T_{MA} or T_{RD}; Table 3) for many of the sulfides fall around 2.7 Ga. Typically, in the absence of an age regression and with their very low Re/Os ratios, these model ages would suggest diamond formation around 2.7 Ga rather than the 3.52 Ga isochron age. However, this younger age can be ruled out because the isochron is a statistically valid regression treatment of the data and is supported by two- or three-point internal isochrons on five separate diamonds. The three sulfides from diamond PD4 are the most constraining in this regard since any 2.7 Ga line misses at least one of the inclusions. Even so, excluding PD4 entirely from the regression does not change the age and initial ratio significantly. Also, older Re–Os model ages are given by some of the harzburgites (Table 4) and corroborated by sulfides in mantle olivines (Aulbach et al. 2004; see Fig. 9 and discussion below). Thus, the most likely interpretation of the data is that the main group of sulfides formed in the Paleoarchean, with a preferred age of 3.52 ± 0.17 Ga and an initial ^{187}Os/^{188}Os ratio of 0.1093 ± 0.0001, which is 6% elevated ($\gamma_{Os} = +6$) compared to that of the primitive mantle at 3.5 Ga (0.1035; Meisel et al. 2001). The elevated initial Os isotopic composition of this isochron explains the young model ages, since the model ages are calculated on the assumption of a bulk silicate Earth initial Os isotopic composition.

Inclusions off the isochron

The remaining eight sulfides, all from less well documented rough diamonds (PA series), scatter more widely. In particular, three sulfides (PA91a, PA92a, and PA97a; off scale not plotted) have present-day suprachondritic ^{187}Os/^{188}Os leading to impossible model ages of 6.23, –0.43, and 6.18 Ga, respectively. This requires at least a two-stage evolution and that the sulfides have equilibrated with a protolith that had a significantly elevated ^{187}Os/^{188}Os such as basalt/eclogite, which does not fit with the high Ni and Os contents of these peridotitic sulfides. Together with samples PA89a and PA94a (Fig. 7), they display a range in ^{187}Re/^{188}Os of 0.14–19.8 and with increasing ^{187}Re/^{188}Os they plot increasingly further away from the 3.5 Ga isochron toward more radiogenic compositions. These deviations could potentially be explained by the loss of a fraction of the sample during sample micro-manipulation as shown in the example of single sulfide inclusion fragments with different Cu/Fe and Re/Os analyzed by Richardson et al. (2001). If any unrecovered sulfide had a higher Re/Os than the bulk sulfide, it could also explain the deviation of sample PA93a above the isochron (Fig. 8).

The five high Re/Os samples, PA93a and PA87c cannot be regressed to yield any meaningful ages even for any two data points. They could represent separate population(s) of inclusions and/or diamonds. Except for PD4, they are all from the PA series which has size, color, and morphological differences from the PD series noted above. Sulfide PA87c, for example, plots above the isochron (Fig. 7) and has a Re–Os model age of 2.33 Ga (Table 3). This sulfide was recovered intact making loss of significant amounts of material unlikely. The distinct symmetrical cubo–octahedral form, smooth rather than frosted surfaces and low Re and Os concentration (Fig. 6) of PA87c, support the idea that it represents a separate paragenesis with a different age.

Sulfide PA95a (Fig. 7) is similar to the sulfides conforming to the isochron in its composition, Re and Os contents, and grain morphology but it lies significantly below the isochron. Os isotope heterogeneities in the source environment similar to the suggested explanation for the six low ^{187}Re/^{188}Os sulfides that deviate below the isochron may also be the cause for the deviation of PA95a.

Harzburgite compositions

The harzburgites are unradiogenic with a range in ^{187}Os/^{188}Os of 0.10633–0.11012 and primitive mantle model ages (T_{MA}) and Re-depletion ages (T_{RD}) of 2.8–3.4 Ga and 2.6–3.1 Ga, respectively (Table 4). They do not display correlated Re–Os systematics (Fig. 9). Xenolith PH2 plots close to the 3.5 Ga growth curve for chondritic mantle. The rest of the xenoliths fall between this composition and the composition of the sulfide inclusions but clearly at higher initial Os isotopic compositions than the chondritic mantle at 3.5 Ga. A similar higher-than-chondritic mantle composition can be inferred from sulfide grains enclosed in olivine in mantle xenocrysts and xenoliths from the A154 pipe of the Diavik mine 18 km from the Panda pipe (Fig. 9; Aulbach et al. 2004). The lack of correlated Re–Os systematics in the harzburgite xenoliths could be a function of open system Re–Os behavior since the incorporation of the harzburgites in the lithosphere (e.g., Carlson et al. 1999a; Griffin et al. 2002). In other peridotite suites, open system behavior appears as more scatter around unradiogenic Os isotopic compositions characteristic of old continental lithospheric mantle and toward typically higher Re/Os (e.g., Carlson et al. 2005). In the Panda case, the harzburgites retain their low Re/Os and extend only above a 3.5 Ga chondritic composition which likely indicates mixing with a secondary source of radiogenic Os. Nonetheless, the harzburgites with the least radiogenic Os isotopic composition provide some of the most compelling evidence for a Paleoarchean origin for the lithospheric mantle beneath Panda. In particular, xenolith PH1 has the lowest present day ^{187}Os/^{188}Os (0.1063), well below the Panda sulfide-inclusion bearing diamond initial value (0.1093), and gives the oldest Re-depletion age of 3.1 Ga. This is an absolute minimum age for the melt depletion in these prospective harzburgitic diamond precursors, precluding the possibility of much younger mixing of diamond forming fluids with a chondritic mantle component (e.g., at 2.6 Ga, the youngest Re-depletion age for xenolith PH18).

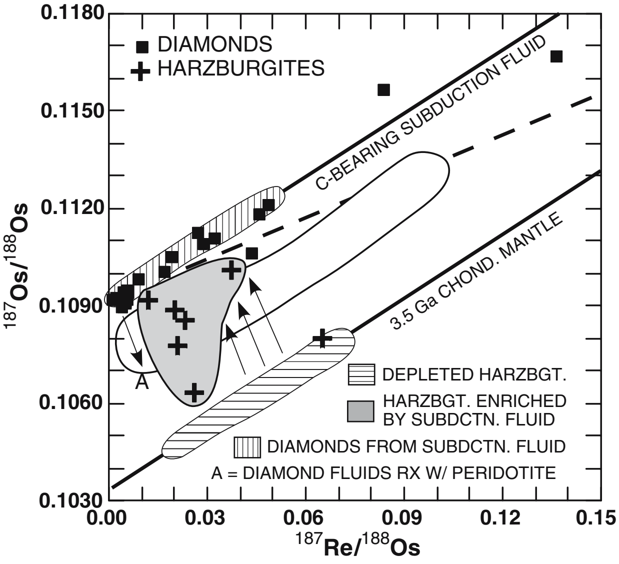

Fig. 9 Re–Os isotopic mixing is shown (*arrows*) between subduction fluids having the radiogenic Os isotopic compositions of the Panda sulfide inclusions (*vertical ruled*) and estimated depleted harzburgites with chondritic initial Os compositions (*horizontal ruled*). *Gray* field of harzburgites enriched by subduction fluids; *white* sulfide inclusions in mantle olivine from the A154 Pipe (Aulbach et al. 2004); *black squares* Panda sulfide inclusions; *crosses* Panda harzburgites. *Solid lines* are 3.5 Ga isochrons. A 2.6 Ga reference isochron from an initial ^{187}Os/^{188}Os of 0.1090 (dashed) is shown for comparison. The mixing raises the isotopic composition of most of the harzburgites and lowers the isotopic composition (*arrow A*) of some of the sulfide inclusions in Panda diamonds

Discussion

A Paleoarchean age for Panda diamonds

Some workers (e.g., Navon 1999; Spetsius et al. 2002) have argued that sulfide inclusions in diamond are protogenetic and as such are incorporated by the growing diamond from its host rock. In this case, the Re–Os system would date the age of sulfide formation and not necessarily constrain diamond growth, which might be substantially younger. The Panda suite of peridotitic sulfide inclusions and harzburgites provides a good test of this hypothesis because it is one of the first suites where inclusions in diamond and the diamond hosts from the same locality have been analyzed for Re–Os. If diamonds formed with mineral inclusions that got their Re and Os from a pre-existing peridotitic protolith, an isochron relationship only would have been obtained if the Re–Os isotope system in the sulfides within the peridotite had been closed since formation and if the discrete Re and Os hosts of the peridotite (e.g., sulfide and/or alloy) were captured in the same modal proportions as they occurred in the peridotite (i.e., minute, discrete, closed sulfide/alloy isotope systems were not brought together or divided at diamond formation). This seems implausible.

The Panda suite has five diamonds that give internal isochrons matching, within errors, the 3.52 Ga age obtained on all 11 inclusions regressed together. As mentioned above, the three inclusions from diamond PD4 are the most constraining since they regress to an age of 3.44 ± 0.58 Ga. For this diamond to have picked up these sulfide inclusions recently from the host harzburgite would require system closure on the millimeter scale in the mantle for more than 3 Ga. This evidently did not occur as is shown by the complete lack of a linear relationship between ^{187}Os/^{188}Os and ^{187}Re/^{188}Os in the harzburgites and the fact that the harzburgites do not overlap with the diamond compositions in their Re–Os systematics (Fig. 9). If younger Panda diamonds simply encapsulated older lithospheric sulfides, then the Panda inclusions analyzed here should plot on a scattered array overlapping the data for the harzburgitic xenoliths (Table 4; Fig. 9) and the sulfide inclusions in olivine analyzed by Aulbach et al. (2004). This study provides clear evidence that the diamonds did not form at a later stage around protogenetic sulfides. Thus the 3.52 ± 0.17 Ga age obtained on peridotitic sulfides is interpreted to be the age of these diamonds. Interestingly, an identical (within errors) age of 3.27 ± 0.34 Ga was obtained on a small subpopulation (<20%) of sulfide grains enclosed in mantle olivines from the A154 pipe of the Diavik mine (Aulbach et al. 2004), thus fully supporting the presence of Paleoarchean lithospheric mantle in this region of the Slave craton. The Aulbach et al. (2004) study also included many sulfide grains (80%) with scattered Re–Os systematics, further reinforcing the idea that sulfide inclusions in diamond do not enclose protogenetic sulfides.

Relationship between the diamonds and the harzburgites

The UDL has an unusually high abundance of subcalcic/high-Cr garnet harzburgite (Griffin et al. 1999; Kopylova and Russell 2000; Menzies et al. 2004) and its high conductance as shown by magnetotelluric studies (Jones et al. 2004) could be due to intergranular graphite indicative of a high C content. These characteristics could make the deeper part of the UDL an important host to harzburgitic diamonds such as the sulfide bearing Panda diamond population studied here and the chromite bearing diamonds of Stachel et al. (2003). As the level of nitrogen aggregation in Panda diamonds reflects an integrated thermal history for 3.5 Ga, the range in T_{MR} up to 1,075°C (as compared to the inferred extent of the UDL down to ~1,000°C on a 53 Ma palaeogeotherm; Menzies et al. 2004) would then require a previously "hotter" geotherm and/or a transient heating event(s) to produce the appropriate N aggregation. The equilibration temperatures–pressures of the Panda harzburgites place them in the diamond stability field within the UDL and the similar petrographic and geochemical character of the harzburgites indicate that all of them have a common origin. Thus, the oldest Re-depletion age of 3.1 Ga for the harzburgites is deemed to be significant as the youngest possible age for the original melt-depletion. The timing of melt depletion is likely older since, as is argued below, there was a post-depletion enrichment of the harzburgite in radiogenic Os. This enrichment would serve to produce anomalously young mantle model ages. Regardless of whether the analyzed diamonds originate in the UDL, or just below the UDL, the UDL must have been in place at, or prior to, diamond formation at 3.5 Ga and the geological history of the UDL, and the Panda harzburgites and diamonds are interpreted to have been linked since that time.

Isotopic mixing and sources for Slave diamonds

Sulfide inclusions and harzburgites with ^{187}Re/^{188}Os as low as that measured for the Panda suite yield accurate initial ^{187}Os/^{188}Os compositions. The 21 main group sulfides clearly show significant isotopic variability that ranges from the six, non-correlated specimens with low Os isotope ratios to the enriched Os isotopic composition of the 14-point isochron initial ratio (Fig. 8). None of the sulfide inclusions have low enough Os isotope ratios to overlap the composition of the harzburgites or chondritic mantle at 3.5 Ga. Thus all inclusion sulfides carry a signature of a diamond-forming fluid with an elevated Os isotopic composition. The harzburgites also show significant scatter to higher than chondritic initial Os isotopic composition (Fig. 9), a signature that is also evident in sulfide inclusions in olivine from the nearby A154 pipe (Aulbach et al. 2004). This suggests that the harzburgites were not a source of the fluid but rather that the harzburgites were affected by this same fluid. Furthermore, the fluid was likely derived external to the lithosphere via a process that imparted a radiogenic Os signature to the fluid with variable degrees of mixing and in multiple pulses. The sinusoidal REE pattern of the harzburgite garnets

(Fig. 1) supports their equilibration with an external source of fluid. The occurrence of inclusions with the lowest ^{187}Os/^{188}Os and ^{187}Re/^{188}Os in the center of some Panda diamonds (e.g., PD6, PD9; Fig. 3a, b) suggests initial diamond crystallization from fluids that have interacted with low ^{187}Os/^{188}Os harzburgites. Other diamonds, with less apparent growth zoning (e.g., PD2, PD10; Fig. 3c, d) crystallized from more isotopically homogeneous, end-member fluid with an elevated ^{187}Os/^{188}Os and higher Re/Os.

As mentioned above, Ni abundances for Panda sulfide inclusions in general follow Os concentration (Fig. 5) but in detail show enough variability to support the idea of multiple pulses of diamond growth under varying degrees of fluid evolution. Some of the diamonds for which multiple inclusions have been analyzed show nearly the same high Ni content for both inclusions (e.g., PD2, PD6, and PA98a) whereas others (PD9 and PD10) each contain one inclusion that has significantly lower Ni. In general, Ni and Re/Os are anti-correlated, as would be expected, but the relationship of the inclusions to diamond growth zones is not always consistent. A plausible explanation would be to have multiple generations of diamond-forming fluids that start producing high Ni sulfides and can evolve (but do not always do so) to a fluid that produces lower Ni sulfides. The Re–Os characteristics of the fluids would vary independently as a function of the extent of source mixing and degree of equilibration with peridotitic protoliths.

Origin of the suprachondritic initial Os isotope compositions

The initial ^{187}Os/^{188}Os ratio of all 21 main group sulfide inclusions is elevated relative to a chondritic mantle at 3.52 Ga (Fig. 9). This requires that the diamond-forming fluids came from a precursor which had a suprachondritic Re/Os ratio for some time prior to the formation of the inclusions. This high Re/Os precursor conceivably could be any of the following: (1) recycled Hadean oceanic crust in the deep mantle, (2) lower mantle equilibrated with a radiogenic outer core, or (3) a fluid derived from subducted sediments and/or basalt.

The suprachondritic ^{187}Os/^{188}Os observed for modern ocean island basalts has been ascribed to the recycling of ocean ridge basalt into the lower mantle on an estimated 800–1,600 million year time-scale (Hauri 2002). In this model the radiogenic Os component of modern OIB reflects the contribution of a recycled crustal pyroxenitic/eclogitic component in the otherwise peridotite-dominated source of the basalt. The peridotitic nature of the sulfide inclusions in the analyzed Panda diamonds and the very depleted harzburgitic compositions of the xenoliths, and in particular the exceptionally low ^{187}Re/^{188}Os of both materials, shows clearly that these materials are not samples of recycled Hadean oceanic crust.

Elevated Os isotopic compositions in the mantle could also be produced if the outer core attained a suprachondritic Re/Os ratio via inner core crystallization and interacted with the overlying lower mantle which was then brought to the upper mantle by plume upwelling (Walker et al. 1995; Brandon et al. 2003). This model has been adopted by Aulbach et al. (2004) to explain the elevated initial ^{187}Os/^{188}Os of 11 sulfides that form their isochron mentioned above. However, a substantial fraction of sulfide grains analyzed by Aulbach et al. (2004) have chondritic ^{187}Os/^{188}Os requiring incorporation of large amounts of chondritic mantle into what would be a heterogeneous plume and dilution of the radiogenic core end member. In addition, models for the ^{187}Os/^{188}Os evolution of the outer core for different modes of inner core crystallization presented by Brandon et al. (2003) suggest a present day outer core ^{187}Os/^{188}Os of ~ 0.143. Assuming that the Re/Os ratio needed to evolve this Os isotopic composition was present by 4.5 Ga, the outer core would have had a ^{187}Os/^{188}Os of 0.106 at 3.5 Ga, substantially lower than the 0.1092 value provided by the Panda sulfide inclusion isochron. Most geophysical models suggest that core crystallization did not begin until post-Archean times (e.g., Stevenson et al. 1983; Buffett et al. 1992; Labrosse et al. 1997; Lister and Buffett 1998; Buffett 2003), making it even less likely that the outer core could have developed sufficiently high ^{187}Os/^{188}Os values by 3.5 Ga to serve as the source of the radiogenic Os in the Panda sulfides.

A third way to obtain elevated Os isotopic compositions in the mantle is shown by modern arc peridotites. Their elevated ^{187}Os/^{188}Os ratios have been attributed to the addition of radiogenic Os from slab-derived fluids or from mantle-wedge melts previously affected by slab-derived fluids (Schiano et al. 1995; Brandon et al. 1996, 1999; Borg et al. 2000; Becker et al. 2001; Widom et al. 2003). Studies of subduction-generated picrites (Woodland et al. 2002) and calc-alkaline lavas (Borg et al. 2000) also point to radiogenic slab-related Os having been introduced into the mantle source region of arc lavas.

There are numerous sources of radiogenic Os in the arc setting such as Mn-nodules (Burton et al. 1999a; Ruiz et al. 1999; McDaniel et al. 2004), the sedimentary component of the slab (Peucker-Ehrenbrink et al. 1995; Pegram and Turekian 1999; Lee et al. 2003), and the oceanic crustal basalt itself (Shirey and Walker

1998) with any attendant enrichments from seafloor hydrothermal vents (Ruiz et al. 1999). Assuming that subducted components in the Archean had similar Re and Os concentration and isotopic composition as modern subduction settings, 1–8% bulk incorporation of subducted materials into depleted peridotite similar to that of the measured harzburgites could explain the elevated initial ^{187}Os/^{188}Os of the sulfide inclusion isochron.

The very low Re contents of the xenoliths would argue that slab-derived fluids were either devoid of Re or that the fluid–solid interaction precluded Re addition. Typically, cratonic peridotite is believed to represent the residue after large extents (30–40%) of melt extraction (e.g., Boyd 1989). Such extensive mantle melting would have removed all sulfide (Keays 1995) and carbon from the melt residue leaving harzburgites completely depleted in S, C, and Re. Bulk-mixing of a sediment containing 0.125 ppb Re which is within the range for present day sediments (Peucker-Ehrenbrink et al. 1995; Lee et al. 2003) and a harzburgite devoid of Re would necessitate a mixing ratio of 90/10 (harzburgite/sediment) to yield the average Re content (0.0125 ppb) of the Panda harzburgites. Fe–Mn nodules which have even lower Re contents than pelagic sediments (McDaniel et al. 2004) could also effectively raise the Re content to the level observed in the xenoliths while imparting the required radiogenic character.

Burton et al. (1999b) showed that the Os isotope composition of pre-existing interstitial sulfide in lherzolite may be overprinted by that of secondary fluids. If the Os isotope composition of the sulfides is determined by the extent of Os exchange between the metasomatic fluid and sulfides or Ir–Os alloys in the harzburgite protoliths, then the isotopic composition of the sulfide inclusions would be dependent on the local fluid/rock ratio (which may have been slightly different at each site of diamond formation). The measured isochron relationship would have been produced by sulfide inclusions that are all formed from the most fluid-rich end-member whereas the inclusions with lower ^{187}Os/^{188}Os formed from fluids whose isotopic composition was lowered slightly by interaction with harzburgite Os (Fig. 9). Based on the location of the sulfide inclusions with the lowest ^{187}Os/^{188}Os in the center of the diamonds (Fig. 3), fluids interacting to a relatively higher degree with harzburgite formed the first generation of diamond growth followed by more enriched and homogeneous fluids with a stronger subduction component. Such interaction could also explain the range in ^{187}Os/^{188}Os at low Re/Os ratio observed in the Panda harzburgites (Fig. 9) and the sinusoidal REE pattern of the harzburgite garnets (Fig. 1). This subduction fluid model provides a way to reintroduce carbon and sulfur to the peridotite depleted from initial melt extraction and provides an explanation for the high nitrogen content of the Panda diamonds which are more like eclogitic diamonds in their nitrogen content compared to peridotitic diamonds worldwide (Fig. 2).

If the elevated ^{187}Os/^{188}Os provided by the sulfide isochron is assumed to represent the Os isotopic composition of the fluid component, a ^{187}Re/^{188}Os of 3.5 would be required to generate this isotopic composition from chondritic mantle in 100 million years. Some komatiites have ^{187}Re/^{188}Os this low, but most komatiites and essentially all basalts and sediments have much higher Re/Os (Shirey and Walker 1998). Thus, all subducted components likely to be present at 3.5 Ga would have sufficiently high ^{187}Os/^{188}Os to contribute to the elevated Os isotopic composition observed for the Panda sulfides.

Implications for Slave craton formation and evolution

In theory, the ultra-depleted layer (UDL) could have formed significantly before 3.5 Ga in response to an Eoarchean crust formation event (e.g., Bowring et al. 1989). However, the model age data for Panda harzburgites provide no clear evidence for such an early formation. The near chondritic ^{187}Os/^{188}Os at 3.5 Ga for xenolith PH2 (Fig. 9) may indicate melt-depletion and harzburgite formation from a chondritic reservoir at that time or it could be a mixture between an even older depleted peridotite and a small amount of slab fluid. The very low Re content of the xenoliths (Table 4) imply that not enough Re has been added to the xenoliths to significantly overprint this melt depletion. Assuming a formation age of about 3.5 Ga for the harzburgites and that the ^{187}Os/^{188}Os ratios of the xenoliths are supported by their ^{187}Re/^{188}Os ratios yields a range in initial γ_{Os} of + 1.0 to + 5.2 that approaches the initial Os isotope composition of the sulfide inclusions (Fig. 9). If melt depletion occurred much earlier than 3.5 Ga, such as at 4 Ga, it would be fortuitous that all the xenoliths have suprachondritic ^{187}Os/^{188}Os ratios at 3.5 Ga (Fig. 9) and it is considered unlikely that the harzburgites could predate the diamonds by more than some 100 million years. In the subsequent discussion, we assume that the age of the UDL is given by the 3.5 Ga isochron on the Panda harzburgitic diamonds; in any case our data and that of Aulbach et al. (2004; 3.2 Ga age) establish the UDL as significantly older than the circa 2.6 Ga age of tectonism and magmatism that affected much of the western Slave craton and produced the juvenile crust of the eastern Slave craton (Davis et al. 2003a, b). Thus the existence of an ancient, cold, shallow portion of mantle lithosphere with the characteristics of the UDL preserved within the mantle keel of the Slave craton 100 km east of the Central Slave Basement Complex and well within the eastern Slave arc (e.g., Davis et al. 2003b) places constraints on how the craton started to form and evolved to the Neoarchean.

The UDL could represent the sub-arc mantle at a convergent margin as suggested by Griffin et al. (1999, 2003). We view its 3.5 Ga age to indicate that it was a 3.5 Ga convergent margin that created the UDL perhaps along with the nascent rocks of the Central Slave Basement Complex itself. If, as argued above, the UDL and harzburgitic diamond formation occurred close in time through subduction metasomatism of sub-arc mantle, diamond formation would be placed within a subduction setting rather than invoking the involvement of a mantle plume. This subduction model is fully supported by the Re–Os isotopic systematics of the sulfide inclusions that have subduction-fluid signatures (Fig. 9) and the need for low pressure melting to produce harzburgitic garnet of an appropriately high Cr/Al ratio (Takahashi 1986; Bulatov et al. 1991; Canil and Wei 1992; Tronnes et al. 1992; Stachel et al. 1998). Subduction beneath the UDL could have contributed fluids for diamond formation similar to the model proposed by Kesson and Ringwood (1989). If these fluids were high in Si, they could also be responsible for the high orthopyroxene/olivine ratios observed in the harzburgite xenoliths (Kesson and Ringwood 1989; Kelemen et al. 1998) and the typical LIL element enrichments of these fluids could have produced the sinusoidal $\mathrm{REE_N}$ patterns observed in the harzburgitic garnets. Co-crystallization of diamonds and their sulfide inclusions would have occurred as the fluids became sufficiently reduced and S-saturated (see similar proposal by Bell et al. 2003). The model presented in this paper predicts that much of the central Slave cratonic lithosphere and its harzburgitic diamonds could have formed within a short time-span of some 100 million years. If the UDL were the hanging wall in a subduction setting, this could explain the absence of eclogite in the UDL, but the presence of eclogite stratigraphically below the UDL (Pearson et al. 1999c; Gurney et al. 2003).

The nucleation of the Kaapvaal craton of southern Africa and the origin of its harzburgitic diamonds also has been ascribed to Paleoarchean to Mesoarchean subduction tectonics (Shirey et al. 2002, 2004). Large volumes of differentiated silicic crust that dominate most cratons can be produced in a subduction regime whereas mantle plumes have neither in the past nor in the present produced crustal sections compositionally similar to the Si-rich, Mg-poor rocks that dominate Archean continental crust (Shirey et al. 2004). Jordan (1979, 1981, 1988) in explaining the development of the continental tectosphere points to the mantle wedge above a subduction zone as the only tectonic regime to offer sustained mantle melting and depletion in a setting where compressional tectonics can thicken the lithospheric mantle.

The 3.5 Ga ultra-depleted layer (UDL) can be interpreted as part of the mantle keel to the Central Slave Basement Complex crust that had translated with it and is now situated under the location of the Panda kimberlite in the eastern Slave arc. This would be an indication that the eastward dipping suture between the Central Slave Basement Complex and the eastern Slave arc (e.g., Bleeker 2003; Davis et al. 2003b), first proposed for the crust on the basis of the Nd isotopic composition of granitoids (Davis and Hegner 1992), continues into the lithospheric mantle. How the eastern Slave arc terrane could be created with a piece of old lithosphere in place underneath it is difficult to understand. However, if the western and eastern portions of the Slave craton were only brought together after the end of plutonic activity in the Slave craton at 2,580 Ma, then the UDL would not need to have been traversed by the fluids and melts that advected heat and volatiles into the crust to cause the plutonic activity that occurred between 2,630 and 2,580 Ma. Unfortunately, this scenario is not supported by the 2,680–2,690 Ma supracrustal cover sequences extending across the suture and the significant post 2,680 Ma magmatic activity in both halves of the craton (e.g., Bleeker 2003; Davis et al. 2003b) that suggest that the eastern and western Slave have been together since that time (Bleeker 2001). Thus the preservation of the UDL and the Panda diamonds becomes a more complex geologic matter. Although Davis et al. (2003b) have made the suggestion (in the absence of direct diamond ages) that the diamonds from the Slave craton should be 2.6 Ga or younger in age, data for the Panda suite presented here show that there may be a significant diamond population in the Slave craton that is older and has little to do with the 2.5–2.7 Ga tectonothermal events marking the stabilization of the Slave craton.

Conclusions

Sulfide bearing diamonds from the Panda kimberlite pipe have lower degrees of nitrogen aggregation for a given nitrogen content than silicate bearing diamonds and a higher nitrogen content than chromite bearing diamonds. These characteristics suggest an origin in the coolest portion of the Slave craton lithospheric mantle such as the ultra-depleted layer (UDL).

An age of 3.52 ± 0.17 Ga has been obtained on 11 inclusions from five diamonds that give coherent internal isochrons. Unfortunately, the extremely low ^{187}Re/^{188}Os ratios and their limited range do not permit a more precise age. Nonetheless, this age coupled with the N aggregation systematics of the diamonds firmly date the UDL as Paleoarchean. A substantial portion of the suite of sulfides falls at lower ^{187}Os/^{188}Os than the isochron initial. Most Panda peridotitic sulfide inclusions crystallized from a source fluid with a ^{187}Os/^{188}Os well above that of chondritic mantle at 3.5 Ga. The harzburgites have even lower ^{187}Os/^{188}Os, the lowest being close to chondritic mantle. The complete lack of overlap shows that these sulfide inclusions cannot be protogenetic with respect to the diamond hosts. The range in isotopic composition of the harzburgites supports a model where fluids with radiogenic Os were introduced into and interacted with depleted harzburgite to form the source of the Panda diamonds. The colinearity of the sulfides that form the isochron indicates that these samples had the same initial Os isotopic composition, and were derived from a well-mixed fluid. These fluids were responsible for raising the isotopic composition of the harzburgites to values higher than chondritic. The most plausible setting consistent with these features is in a Paleoarchean subduction zone where the fluids were introduced from the slab into depleted harzburgite in the wedge forming the earliest portions of the Slave craton lithosphere. The 3.5 Ga diamond ages suggest that the UDL may have been part of the mantle keel to the Central Slave Basement Complex. Its current location beneath the eastern Slave arc suggests that it was not affected by the 2.5–2.7 Ga igneous activity marking the stabilization of the Slave craton.

Acknowledgments Discussions with Graham Pearson and Mark Schmitz are greatly appreciated. The authors are grateful to BHP Diamonds and to the Diamond Trading Company (a De Beers Group Company) for making diamonds available for study. Mary Horan and Tim Mock are thanked for their help in the DTM chemistry and mass spectrometry labs (respectively). Judith Milledge at the University College London is thanked for her continuous support over the years with ideas and software for the reduction of FTIR absorption data. Frank Spear assisted in calculating garnet compositions. Bill Davis and Wouter Bleeker generously shared their perspectives on Slave craton evolution. The manuscript benefited from the careful reviews of Mark Schmitz and Maya Kopylova. This work was supported in the USA chiefly by the Carnegie Institution of Washington and NSF EAR Continental Dynamics Grant 9526840 and in South Africa by the Department of Geological Sciences of the University of Cape Town and the National Research Foundation.

References

Ahmed AH, Arai S (2003) Platinum-group minerals in podiform chromitites of the Oman ophiolite. Can Mineral 41:597–616

Aulbach S, Griffin WL, Pearson NJ, O'Reilly SY, Kivi K, Doyle BJ (2004) Mantle formation and evolution, Slave craton: constraints from HSE abundances and Re-Os isotope systematics of sulfide inclusions in mantle xenocrysts. Chem Geol 208:61–88

Becker H, Shirey SB, Carlson RW (2001) Effects of melt percolation on the Re-Os systematics of peridotites from a Paleozoic convergent plate margin. Earth Planet Sci Lett 188:107–121

Bell DR, Gregoire M, Grove TL, Chatterjee N, Bowring SA (2003) Silica and carbon deposition in Kimberley peridotites. In: 8th International Kimberlite Conference, extended abstracts. Victoria, BC, Canada, p FLA_0289

Bleeker W (2001) The ca. 2680 Ma Raquette Lake formation and correlative units across the Slave Province, Northwest Territories: evidence for a craton-scale overlap sequence. Geological Survey of Canada, Current Research 2001-C7:11

Bleeker W (2003) The late Archean record; a puzzle in ca. 35 pieces. Lithos 71:99–134

Borg LE, Brandon AD, Clynne MA, Walker RJ (2000) Re-Os isotopic systematics of primitive lavas from the Lassen region of the Cascade arc, California. Earth Planet Sci Lett 177:301–317

Bowring SA, Williams IS, Compston W (1989) 3.96 Ga gneisses from the Slave Province, Northwest Territories, Canada; with supplementary data 89–17. Geology 17:971–975

Boyd FR (1989) Compositional distinction between oceanic and cratonic lithosphere. Earth Planet Sci Lett 96:15–26

Brandon AD, Creaser RA, Shirey SB, Carlson RW (1996) Osmium recycling in subduction zones. Science 272:861–864

Brandon AD, Becker H, Carlson RW, Shirey SB (1999) Isotopic constraints on time scales and mechanisms of slab material transport in the mantle wedge: evidence from the Simcoe mantle xenoliths, Washington, USA. Chem Geol 160:387–407

Brandon AD, Walker RJ, Puchtel IS, Becker H, Humayun M, Revillon S (2003) ^{186}Os/^{188}Os systematics of Gorgona Island komatiites; implications for early growth of the inner core. Earth Planet Sci Lett 206:411–426

Brenan JM (2002) Re-Os fractionation in magmatic sulfide melt by monosulfide solid solution. Earth Planet Sci Lett 199:257–268

Brey GP, Kohler T (1990) Geothermobarometry in four-phase lherzolites ii. New thermometers and practical assessment of existing thermometers. J Petrol 31:1353–1378

Buffett BA (2003) The thermal state of Earth's core. Science 299:1675–1677

Buffett BA, Huppert HE, Lister JR, Woods AW (1992) Analytical model for solidification of the Earth's core. Nature 356:329–331

Bulanova GP, Griffin WL, Ryan CG, Shestakova OY, Barnes SJ (1996) Trace elements in sulfide inclusions from Yakutia diamonds. Contrib Mineral Petrol 124:111–125

Bulatov V, Brey GP, Foley SF (1991) Origin of low-Ca, high-Cr garnets by recrystallization of low-pressure harzburgites. In: 5th International Kimberlite Conference, 2/91. CRPM Special Publication, Araxa, Brazil, pp 29–31

Burton KW, Bourdon B, Birck J-L, Allegre CJ, Hein JR (1999a) Osmium isotope variations in the oceans recorded by Fe-Mn crusts. Earth Planet Sci Lett 171:185–197

Burton KW, Schiano P, Birck J-L, Allegre CJ (1999b) Osmium isotope disequilibrium between mantle minerals in a spinel-lherzolite. Earth Planet Sci Lett 172:311–322

Canil D, Wei K (1992) Constraints on the origin of mantle-derived low-Ca garnets. Contrib Mineral Petrol 109:421–430

Carlson RW, Irving AJ (1994) Depletion and enrichment history of subcontinental lithospheric mantle: an Os, Sr, Nd and Pb isotopic study of ultramafic xenoliths from the northwestern Wyoming Craton. Earth Planet Sci Lett 126:457–472

Carlson JA, Kirkley MB, Thomas EM, Hillier WD (1999a) Recent Canadian kimberlite discoveries. In: Gurney JJ, Gurney JL, Pascoe MD, Richardson SH (eds) The J. B. Dawson volume–proceedings of the 7th International Kimberlite Conference, Cape Town. Red Roof Design, Cape Town, pp 81–89

Carlson RW, Pearson DG, Boyd FR, Shirey SB, Irvine G, Menzies AH, Gurney JJ (1999b) Re-Os systematics of lithospheric peridotites: implications for lithosphere formation and preservation. In: Gurney JJ, Gurney JL, Pascoe MD, Richardson SH (eds) The J. B. Dawson volume–proceedings of the 7th International Kimberlite Conference, Cape Town. Red Roof Design, Cape Town, pp 99–108

Carlson RW, Pearson DG, James DE (2005) Physical, chemical and chronological characteristics of continental mantle. Rev Geophys 43:RG1001. DOI 10.1029/2004RG000156

Creaser RA, Grutter HS, Carlson JA, Crawford BB (2004) Macrocrystal phlogopite Rb/Sr dates for the Ekati property kimberlites, Slave Province, Canada; evidence for multiple intrusive episodes in the Paleocene and Eocene. Lithos 76:399–414

Davis WJ, Hegner E (1992) Neodymium isotopic evidence for the accretionary development of the late Archean Slave Province. Contrib Mineral Petrol 111:493–503

Davis WJ, Canil D, MacKenzie JM, Carbno GB (2003a) Petrology and U-Pb geochronology of lower crustal xenoliths and the development of a craton, Slave Province, Canada. Lithos 71:541–573

Davis WJ, Jones AG, Bleeker W, Grutter H (2003b) Lithosphere development in the Slave craton: a linked crustal and mantle perspective. Lithos 71:575–589

Deines P, Harris JW (1995) Sulfide inclusion chemistry and carbon isotopes of African diamonds. Geochim Cosmochim Acta 59:3173–3188

Dyck DR, Oshust PA, Carlson JA, Nowicki TE, Mullins MP (2004) Effective resource estimates for primary diamond deposits from the Ekati diamond mine, Canada. Lithos 76:317–335

Ebel DS, Naldrett AJ (1997) Crystallization of sulfide liquids and the interpretation of ore composition. Can J Earth Sci 34:352–365

Finnerty AA, Boyd FR (1984) Evaluation of thermobarometers for garnet peridotites. Geochim Cosmochim Acta 48:15–27

Fleet ME, Crocket JH, Liu M, Stone WE (1999) Laboratory partitioning of platinum-group elements (PGE) and gold with application to magmatic sulfide-PGE deposits. Lithos 47:127–142

Foster JG, Lambert DD, Frick LR, Maas R (1996) Re-Os isotopic evidence for genesis of Archean nickel ores from uncontaminated komatiites. Nature 382:703–706

Griffin WL, Gurney JJ, Ryan CG (1992) Variations in trapping temperatures and trace elements in peridotite-suite inclusions from African diamonds: evidence for two inclusion suites and implications for lithosphere stratigraphy. Contrib Mineral Petrol 110:1–15

Griffin WL, Doyle BJ, Ryan CG, Pearson NJ, O'Reilly SY, Davies R, Kivi K, van Achterbergh E, Natapov LM (1999) Layered mantle lithosphere in the Lac de Gras area, Slave craton; composition, structure and origin. J Petrol 40:705–727

Griffin WL, Spetsius ZV, Pearson NJ, O'Reilly SY (2002) In situ Re-Os analysis of sulfide inclusions in kimberlitic olivine; new constraints on depletion events in the Siberian lithospheric mantle. Geochem Geophys Geosyst–G^3 3:25

Griffin WL, O'Reilly SY, Abe N, Aulbach S, Davies RM, Pearson NJ, Doyle BJ, Kivi K (2003) The origin and evolution of Archean lithospheric mantle. Precambrian Res 127:19–41

Gurney JJ (1989) Diamonds. In: Ross J, Jaques AL, Ferguson J, Green DH, O'Reilly SY, Danchin RV, Janse AJA (eds) Kimberlites and related rocks, Special Publication Number 14, vol. 2. Geological Society of Australia, Sydney, N.S.W., Australia, pp 935–965

Gurney JJ, Switzer GS (1973) The discovery of garnets closely related to diamonds in the Finsch pipe, South Africa. Contrib Mineral Petrol 39:103–116

Gurney JJ, Westerlund K, Carlson RW, Shirey SB (2003) Mineral compositions and Re-Os isotope systematics of harzburgite nodules from the Panda kimberlite, Slave craton. In: 8th International Kimberlite Conference, extended abstracts. Victoria, BC Canada, p FLA_0138

Harley SL (1984) An experimental study of the partitioning of Fe and Mg between garnet and orthopyroxene. Contrib Mineral Petrol 86:359–373

Hauri EH (2002) Osmium isotopes and mantle convection. Phil Trans Roy Soc A: Math Phys Eng Sci 360:2371–2382

Hauri EH, Wang J, Pearson DG, Bulanova GP (2002) Microanalysis of δ^{13}C, δ^{15}N, and N abundances in diamonds by secondary ion mass spectrometry. Chem Geol 185:149–163

Hoal KEO, Hoal BG, Erlank AJ, Shimizu N (1994) Metasomatism of the mantle lithosphere recorded by rare earth elements in garnets. Earth Planet Sci Lett 126:303–313

Irvine G (2002) Time constraints on the formation of lithospheric mantle beneath cratons: a Re-Os isotope and platinum group element study of peridotite xenoliths from northern Canada and Lesotho. Unpublished Ph.D. thesis, University of Durham, Durham, UK, 384 pp

Irvine G, Pearson DG, Kjarsgaard BA, Carlson RW, Kopylova MG, Dreibus G (2003) A Re-Os isotope and PGE study of kimbelite-derived peridotite xenoliths from Somerset Island and a comparison to the Slave and Kaapvaal cratons. Lithos 71:461–488

Jones AG, Lezaeta P, Ferguson IJ, Chave AD, Evans RL, Garcia X, Spratt J (2004) The electrical structure of the Slave craton. Lithos 71:505–527

Jordan TH (1979) Mineralogies, densities and seismic velocities of garnet lherzolites and their geophysical implications. In: Boyd FR, Meyer HOA (eds) The mantle sample; inclusions in kimberlites and other volcanics. American Geophysical Union, Washington, DC, pp 1–14

Jordan TH (1981) Continents as a chemical boundary layer. Philos Trans R Soc Lond A 301:359–373

Jordan TH (1988) Structure and formation of the continental tectosphere. J Petrol Spec Lithosphere Issue: 11–37

Karup-Moller S, Mackovicky E (1998) The phase system Fe-Ni-S at 900°C. Neues Jahrb Min Monatschifte 1998:373–384

Keays RR (1995) The role of komatiitic and picritic magmatism and S-saturation in the formation of ore deposits. Lithos 34:1–18

Kelemen PB, Hart SR, Bernstein S (1998) Silica enrichment in the continental upper mantle via melt/rock reaction. Earth Planet Sci Lett 164:387–406

Kennedy CS, Kennedy GC (1976) The equilibrium boundary between graphite and diamond. J Geophys Res 81:2467–2470

Kesson S, Ringwood AE (1989) Slab-mantle interactions 2. The formation of diamonds. Chem Geol 78:97–118

Kopylova MG, Russell JK (2000) Chemical stratification of cratonic lithosphere; constraints from the northern Slave craton, Canada. Earth Planet Sci Lett 181:71–87

Labrosse S, Poirier J-P, Le Mouel J-L (1997) On cooling of the Earth's core. Phys Earth Planet Inter 99:1–17

Lee C-TA, Wasserburg GJ, Kyte FT (2003) Platinum-group elements (PGE) and rhenium in marine sediments across the Cretaceous-Tertiary boundary; constraints on Re-PGE transport in the marine environment. Geochim Cosmochim Acta 67:655–670

Lister JR, Buffett BA (1998) Stratification of the outer core at the core-mantle boundary. Phys Earth Planet Inter 105:5–19

Ludwig KR (2003) Isoplot 3.0: a geochronological toolkit for Microsoft Excel, Special Publication Number 4. Berkeley Geochronology Center, Berkeley, CA, 70 pp

MacGregor ID (1974) The system MgO-Al_2O_3-SiO_2; solubility of Al_2O_3 in enstatite for spinel and garnet peridotite compositions. Am Mineral 59:110–119

McDaniel DK, Walker RJ, Hemming SR, Horan MF, Becker H, Grauch RI (2004) Sources of osmium to the modern oceans: new evidence from the ^{190} Pt-^{186} Os system. Geochim Cosmochim Acta 68:1243–1252

McDonough WF, Sun SS (1995) The composition of the Earth. Chem Geol 120:223–253

Meisel T, Walker RJ, Irving AJ, Lorand J-P (2001) Osmium isotopic compositions of mantle xenoliths; a global perspective. Geochim Cosmochim Acta 65:1311–1323

Menzies AH, Westerlund K, Grutter H, Gurney JJ, Carlson JA, Fung A, Nowicki T (2004) Peridotitic mantle xenoliths from kimberlites on the Ekati diamond mine property, NWT, Canada: major element compositions and implications for the lithosphere beneath the central Slave craton. Lithos 77:395–412

Morgan JW (1986) Ultramafic xenoliths: clues to Earth's late accretionary history. J Geophys Res 91:12375–312387

Naldrett AJ (1989) Magmatic sulfide deposits, 14. Oxford University Press, New York, 186 pp

Navon O (1999) Diamond formation in the Earth's mantle. In: Gurney JJ, Gurney JL, Pascoe MD, Richardson SH (eds) The P. H. Nixon volume–proceedings of the 7th International Kimberlite Conference, Cape Town. Red Roof Design, Cape Town, pp 584–604

Nickel KG, Green DH (1985) Empirical geothermobarometry for garnet peridotites and implications for the nature of the lithosphere, kimberlites and diamonds. Earth Planet Sci Lett 73:158–170

Nowicki T, Crawford BB, Dyck DR, Carlson JA, McElroy R, Oshust P, Helmstaedt H (2004) The geology of kimberlite pipes of the Ekati property, Northwest Territories, Canada. Lithos 76:1–27

O'Neill HSC, Wood BJ (1979) An experimental study of Fe-Mg partitioning between garnet and olivine and its calibration as a geothermometer. Contrib Mineral Petrol 70:59–70

Pearson DG, Shirey SB (1999) Isotopic dating of diamonds. In: Lambert David D, Ruiz J (eds) Application of radiogenic isotopes to ore deposit research and exploration, 12. Society of Economic Geologists, Boulder, CO, United States, pp 143–171

Pearson DG, Carlson RW, Shirey SB, Boyd FR, Nixon PH (1995a) Stabilisation of Archean lithospheric mantle; a Re-Os isotope study of peridotite xenoliths from the Kaapvaal craton. Earth Planet Sci Lett 134:341–357

Pearson DG, Shirey SB, Carlson RW, Boyd FR, Pokhilenko NP, Shimizu N (1995b) Re-Os, Sm-Nd, and Rb-Sr isotope evidence for thick Archean lithospheric mantle beneath the siberian craton modified by multistage metasomatism. Geochim Cosmochim Acta 59:959–977

Pearson DG, Shirey SB, Harris JW, Carlson RW (1998) Sulfide inclusions in diamonds from the Koffiefontein kimberlite, S. Africa: constraints on diamond ages and mantle Re-Os systematics. Earth Planet Sci Lett 160:311–326

Pearson DG, Shirey SB, Bulanova GP, Carlson RW, Milledge HJ (1999a) Dating and paragenetic distinction of diamonds using the Re-Os isotope system; application to some Siberian diamonds. In: Gurney JJ, Gurney JL, Pascoe MD, Richardson SH (eds) The P. H. Nixon volume–proceedings of the 7th International Kimberlite Conference, Cape Town. Red Roof Design, Cape Town, pp 637–643

Pearson DG, Shirey SB, Bulanova GP, Carlson RW, Milledge HJ (1999b) Re-Os isotope measurements of single sulfide inclusions in a Siberian diamond and its nitrogen aggregation systematics. Geochim Cosmochim Acta 63:703–711

Pearson NJ, Griffin WL, Doyle BJ, O'Reilly SY, van Achterbergh E, Kivi K (1999c) Xenoliths from kimberlite pipes of the Lac de Gras area, Slave craton, Canada. In: Gurney JJ, Gurney JL, Pascoe MD, Richardson SH (eds) The P. H. Nixon volume–proceedings of the 7th International Kimberlite Conference, Cape Town. Red Roof Design, Cape Town, pp 644–658

Pearson DG, Canil D, Shirey SB (2003) Chapter 7–Mantle samples included in volcanic rocks: xenoliths and diamonds. In: Carlson RW (ed) Treatise on geochemistry: vol. 2, the Mantle. Elsevier, New York, pp 171–277

Pegram WJ, Turekian KK (1999) The osmium isotopic composition change of Cenozoic sea water as inferred from a deep-sea core corrected for meteoritic contributions. Geochim et Cosmochim Acta 63:4053–4058

Peucker-Ehrenbrink B, Ravizza G, Hofmann AW (1995) The marine $^{187}Os/^{188}Os$ record of the past 80 million years. Earth Planet Sci Lett 130:155–167

Puchtel I, Brugmann G, Hofmann A (2001) ^{187}Os-enriched domain in an Archean mantle plume: evidence from 2.8 Ga komatiites of the Kostomuksha greenstone belt, NW Baltic Shield. Earth Planet Sci Lett 186:513–526

Richardson SH, Gurney JJ, Erlank AJ, Harris JW (1984) Origin of diamonds in old enriched mantle. Nature 310:198–202

Richardson SH, Shirey SB, Harris JW, Carlson RW (2001) Archean subduction recorded by Re-Os isotopes in eclogitic sulfide inclusions in Kimberley diamonds. Earth Planet Sci Lett 191:257–266

Richardson SH, Shirey SB, Harris JW (2004) Episodic diamond genesis at Jwaneng, Botswana, and implications for Kaapvaal craton evolution. Lithos 77:143–154

Robb LJ, Knoll AH, Plumb KA, Shields GA, Strauss H, Veizer J (2004) Chapter 9. The Precambrian: the Archean and Proterozoic eons. In: A geological time scale 2004. Cambridge University Press, New York, p 589

Rudnick RL, Nyblade AA (1999) The thickness and heat production of Archean lithosphere; constraints from xenolith thermobarometry and surface heat flow. In: Fei Y, Bertka CM, Mysen BO (eds) Mantle petrology: field observations and high pressure experimentation, special publication number 6. Geochemical Society, pp 3–12

Ruiz J, McCandless TE, Helmstaedt HH (1999) Re-Os model ages for eclogite xenoliths from the Colorado Plateau. In: Gurney JJ, Gurney JL, Pascoe MD, Richardson SH (eds) The P. H. Nixon volume–proceedings of the 7th International Kimberlite Conference, Cape Town. Red Roof Design, Cape Town, pp 736–740

Ryan CG, Griffin WL, Pearson NJ (1996) Garnet geotherms; pressure-temperature data from Cr-Pyrope garnet xenocrysts in volcanic rocks. J Geophys Res B, Solid Earth Planet 101:5611–5625

Schiano P, Clocchiatti R, Shimizu N, Maury RC, Jochum KP, Hofmann AW (1995) Hydrous, silica-rich melts in the subarc mantle and their relationship with erupted arc lavas. Nature 377:595–600

Schulze DJ (1995) Low-Ca garnet harzburgites from Kimberley, South Africa; abundance and bearing on the structure and evolution of the lithosphere. J Geophys Res B, Solid Earth Planet 100:12513–512526

Shimizu N, Richardson SH (1987) Trace element abundance patterns of garnet inclusions in peridotite-suite diamonds. Geochim Cosmochim Acta 51:755–758

Shirey SB, Walker RJ (1995) Carius tube digestion for low-blank rhenium-osmium analysis. Anal Chem 34:2136–2141

Shirey SB, Walker RJ (1998) The Re-Os isotope system in cosmochemistry and high-temperature geochemistry. Annu Rev Earth Planet Sci. 26:423–500

Shirey SB, Pearson DG, Richardson SH, Harris JW, Carlson RW (2000) Application of Re-Os microchemistry to sulfide inclusions in diamond and implications for Archean craton evolution. Eos Trans Am Geophys Union 81:S428

Shirey SB, Harris JW, Richardson SH, Fouch MJ, James DE, Cartigny P, Deines P, Viljoen F (2002) Diamond genesis, seismic structure, and evolution of the Kaapvaal-Zimbabwe craton. Science 297:1683–1686

Shirey SB, Richardson Stephen H, Harris JW (2004) Integrated models of diamond formation and craton evolution. Lithos 77:923–944

Sobolev NV, Laurent'ev Yu G, Pokhilenko NP (1973) Chrome-rich garnets from the kimberlites of Yakutia and their paragenesis. Contrib Mineral Petrol 40:39–52

Spetsius ZV, Belousova EA, Griffin WL, O'Reilly SY, Pearson NJ (2002) Archean sulfide inclusions in Paleozoic zircon megacrysts from the Mir kimberlite, Yakutia; implications for the dating of diamonds. Earth Planet Sci Lett 199:111–126

Stachel T, Harris JW (1997) Diamond precipitation and mantle metasomatism; evidence from the trace element chemistry of silicate inclusions in diamonds from Akwatia, Ghana. Contrib Mineral Petrol 129:143–154

Stachel T, Viljoen KS, Brey G, Harris JW (1998) Metasomatic processes in lherzolitic and harzburgitic domains of diamondiferous lithospheric mantle; REE in garnets from xenoliths and inclusions in diamonds. Earth Planet Sci Lett 159:1–12

Stachel T, Harris JW, Tappert R, Brey GP (2003) Peridotitic diamonds from the Slave and Kaapvaal cratons–similarities and differences based on a preliminary data set. Lithos 71:489–5003

Stevenson D, Spohn T, Schubert G (1983) Magmatism and thermal evolution of the terrestrial planets. Icarus 54:466–489

Takahashi E (1986) Melting of a dry peridotite KLB-1 up to 14 GPa: implications for the origin of peridotite upper mantle. J Geophys Res 91:9367–9382

Taylor LA, Anand M (2004) Diamonds: time capsules from the Siberian mantle. Chem Erde 64:1–74

Tronnes RG, Canil D, Wei KJ (1992) Element partitioning between silicate minerals and coexisting melts at pressures of 1–27 GPa and implications for mantle evolution. Earth Planet Sci Lett 111:241–255

Walker RJ, Shirey SB, Stecher O (1988) Comparative Re-Os, Sm-Nd and Rb-Sr isotope and trace element systematics for Archean komatiite flows from Munro Township, Abitibi Belt, Ontario. Earth Planet Sci Lett 87:1–12

Walker RJ, Carlson RW, Shirey SB, Boyd FR (1989) Os, Sr, Nd, and Pb isotope systematics of southern African peridotite xenoliths; implications for the chemical evolution of subcontinental mantle. Geochim Cosmochim Acta 53:1583–1595

Walker RJ, Echeverria LM, Shirey SB, Horan MF (1991) Re-Os isotopic constraints on the origin of volcanic rocks, Gorgona Island, Colombia; Os isotopic evidence for ancient heterogeneities in the mantle. Contrib Mineral Petrol 107:150–162

Walker RJ, Morgan JW, Horan MF (1995) ^{187}Os enrichment in some plumes: evidence for core-mantle interaction. Science 269:819–822

Westerlund K (2005) A geochemical study of diamonds, mineral inclusions in diamonds and mantle xenoliths from the Panda kimberlite, Slave craton. Unpublished Ph.D. thesis, University of Cape Town, Cape Town, South Africa, 170 pp

Westerlund K, Hauri EH, Gurney JJ (2003) FTIR absorption and stable nitrogen and carbon isotope microanalysis of mid-Archean diamonds from the Panda kimberlite. In: 8th International Kimberlite Conference, extended abstracts. Victoria, BC Canada, p FLA_0137

Widom E, Kepezhinkas P, Defant M (2003) The nature of metasomatism in the sub-arc mantle wedge: evidence from Re-Os isotopes in Kamchatka peridotite xenoliths. Chem Geol 196:283–306

Woodland SJ, Pearson DG, Thirlwall MF (2002) A platinum group element and Re-Os isotope investigation of siderophile element recycling in subduction zones: comparison of Grenada, Lesser Antilles arc, and the Izu-Bonin arc. J Petrol 43:171–198